Analytica Chimica Acta 674 (2010) 102–109

Contents lists available at ScienceDirect

Analytica Chimica Acta

journal homepage: www.elsevier.com/locate/aca

Non-orthogonal micro-free flow electrophoresis: From theory to design concept

Christopher J. Evenhuis, Victor Okhonin, Sergey N. Krylov*

Department of Chemistry and Center for Research on Biomolecular Interactions, York University, Toronto, Ontario M3J 1P3, Canada

ARTICLE INFO

Article history:
Received 19 May 2010
Received in revised form 28 May 2010
Accepted 1 June 2010
Available online 9 June 2010

Keywords:
Resolution
Electric field strength
Hydrodynamic flow velocity
Electroosmotic mobility
Channel height

ABSTRACT

Micro-free flow electrophoresis (μFFE) is a technique that facilitates continuous separation of molecules in a shallow channel with a hydrodynamic flow and an electric field at an angle to the flow. We recently developed a general theory of μFFE that suggested that an electric field non-orthogonal to the flow could improve resolution. Here, we used computer modeling to study resolution as a function of the electric field strength and the angle between the electric field and the hydrodynamic flow. In addition we used our general theory of μFFE to investigate other important influences on resolution, which include the velocity of the hydrodynamic flow, the height of the separation channel, and the magnitude and direction of the electroosmotic flow. Finally, we propose four designs that could be used to generate non-orthogonal electric fields and discuss their relative merits.

1. Introduction

Chemical synthesis in continuous-flow microreactors (abbreviated to micro-synthesis) is highly attractive for many synthetic applications, due to their unparalleled levels of control and safety. Optimization in micro-synthesis requires analysis of the products. Using present discontinuous batch technologies to analyze the products from continuous synthesis is time consuming and labor intensive and slows the rate at which micro-synthesis reactions can be optimized [1,2]. We propose that this log-jam could be cleared using micro-free flow electrophoresis (μFFE) to continuously separate and analyze the output from continuous-flow microreactors. Continuous collection of analytes is possible in a wide micro-channel with a hydrodynamic flow between two open ends when an electric field causes the separation to be orthogonal to the direction of the flow (see Fig. 1A) [3]. A challenge for μFFE in its current form is to provide baseline resolution of species with similar charge-to-size ratios [4]; this currently limits its practical applicability for combined in-flow synthesis and continuous analysis.

Our previously developed general theory of μFFE [5] challenged the assumption that the best orthogonal resolution would be achieved using an electric field orthogonal to the hydrodynamic flow (as shown in Fig. 1A). The orthogonal resolution, R_S, is defined as the quotient of lateral separation, Δx, and average stream width, w_{av} [6]:

$$R_S = \frac{\Delta x}{w_{av}} = \frac{2\Delta x}{w_1 + w_2} \quad (1)$$

where Δx is measured between the centers of two separated streams and w_1 and w_2 are their widths (Fig. 1B). Our theory showed that a non-orthogonal electric field can greatly improve separation of difficult-to-separate species in the orthogonal direction by increasing the lateral separation by a greater factor than the increase in the average stream width. Our modeling suggests that an improvement in resolution of an order of magnitude is possible using non-orthogonal μFFE. This finding suggests that non-orthogonal μFFE could be suitable for continuous purification of difficult-to-separate analytes. What still needs to be done to make this a reality? Firstly, an understanding of how the parameters in the general equation influence resolution is required. In this work, we address this issue using numerical modeling to identify the major influences on resolution for two groups of species: large slowly diffusing molecules (e.g. biopolymers) and small molecules with large diffusion coefficients (e.g. pharmaceuticals). We show that by optimizing the angle and electric field strength an order of magnitude improvement in resolution can be achieved in comparison with orthogonal μFFE. We also demonstrate how the other parameters, such as hydrodynamic velocity, channel height, and electroosmotic mobility influence the resolution. Secondly, a means of generating non-orthogonal electric fields is needed. Thirdly, a fully functioning non-orthogonal μFFE device is required. The current work creates a solid foundation for this practical effort.

* Corresponding author. Tel.: +1-416-737-2100; fax: +1-416-737-5936.
E-mail address: skrylov@yorku.ca (S.N. Krylov).

0003-2670/$ – see front matter © 2010 Elsevier B.V. All rights reserved.
doi:10.1016/j.aca.2010.06.002

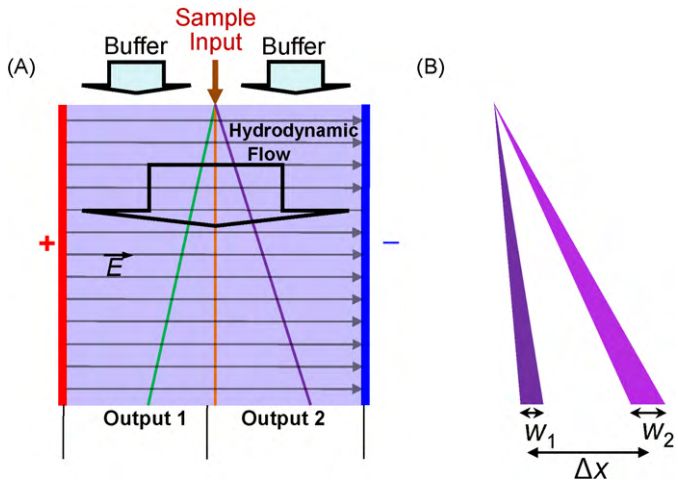

Fig. 1. (A) Schematic of an orthogonal FFE device. The green, orange and purple lines represent the paths taken by negative, neutral and positive molecules, respectively, in the absence of electroosmotic flow. $\vec{E}$ is the vector of the electric field. (B) Shape and trajectory of two separated streams showing their widths, w_1 and w_2, and separation of their stream centers, Δx. (For interpretation of the references to color in text, the reader is referred to the web version of the article.)

2. Results and discussion

2.1. Setup for non-orthogonal μFFE

We propose the following general theoretical setup of μFFE (see Fig. 2). A thin channel has 2 walls in the x–y plane separated by a distance h. The hydrodynamic flow between the walls is in the y direction and has a parabolic flow profile with a maximum velocity in the plane ($z = 0$), equidistant from the two walls. The electric field is assumed to be uniform with a constant strength, $\vec{E}$, acting in the x–y plane. (An arrow above a symbol means that it is a vector.) The electric field makes an angle, φ, with the direction of the hydrodynamic flow and has vector components E_x and E_y projected on the x and y axes, respectively. The resulting electroosmotic flow has corresponding velocity components of $v_{\mathrm{EOF},x}$ and $v_{\mathrm{EOF},y}$. The electroosmotic velocity in the x direction is depth-dependent due to recirculation of the flow caused by the side walls (shown in dark blue) (for interpretation of the references to color in text, the reader is referred to the web version of the article); however, the electroosmotic flow in the y direction is assumed to be constant. A charged molecule placed in the conducting fluid (electrolyte) will experience a combination of an electrostatic force due to the electric field and a frictional force due to its motion relative to the viscous medium; this leads to a constant electrophoretic velocity, $\bar{v}_{\mathrm{ep}}$, parallel to $\vec{E}$. This velocity has x and y components, $v_{\mathrm{ep},x}$ and $v_{\mathrm{ep},y}$, respectively. The magnitude of $\vec{v}_{\mathrm{ep}}$ is directly proportional to the charge of the molecules and inversely proportional to their hydrodynamic radius. Larger molecules carrying small charges move slower than small highly-charged molecules. Molecules carrying an opposite charge are deflected in the opposite direction (see Fig. 1A). The magnitudes of the components of the electrophoretic and electroosmotic velocities are determined by the electric field strength, E, and the angle φ [7]:

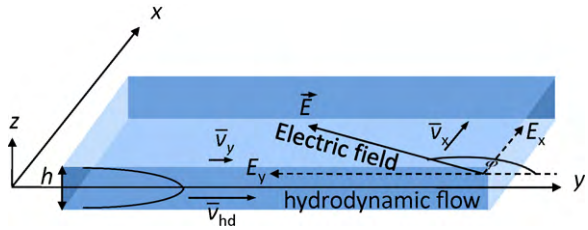

Fig. 2. Schematic diagram defining the geometry on non-orthogonal μFFE. The meanings of the symbols are as follows: $\bar{v}_{\mathrm{hd}}$ is the average velocity of the hydrodynamic flow, $\bar{v}_x$ and $\bar{v}_y$ are components of the average resultant velocity of a species in the direction perpendicular and parallel to the hydrodynamic flow, respectively, $\vec{E}$ is the electric field strength with components E_x and E_y, and φ is the angle between the direction of the hydrodynamic flow and the electric field.

$$\begin{aligned} v_{\mathrm{ep},x} &= \mu_{\mathrm{ep}} E \sin\varphi, \quad v_{\mathrm{EOF},x} = \mu_{\mathrm{EOF}} E \sin\varphi \left(\frac{6z^2}{h^2} - \frac{1}{2}\right) \\ v_{\mathrm{ep},y} &= \mu_{\mathrm{ep}} E \cos\varphi, \quad v_{\mathrm{EOF},y} = \mu_{\mathrm{EOF}} E \cos\varphi \end{aligned} \tag{2}$$

where μ_{EOF} is the electroosmotic mobility, μ_{ep} is the electrophoretic mobility, and h is the height of the separation channel. We emphasize, that the presence of the side walls in the z–y plane results in recirculation of the electroosmotic flow in the x–z plane. At the upper and lower walls of the separation channel ($z = \pm h/2$), $v_{\mathrm{EOF},x} = \mu_{\mathrm{EOF}} E_x$ and at $z = 0$, $v_{\mathrm{EOF},x} = -\mu_{\mathrm{EOF}} E_x/2$. It follows that the average electroosmotic velocity in the x direction is zero. Each of these assumptions is encompassed in our general equation for resolution. Readers interested in how these assumptions are applied in the derivation of our general equation are referred to Supporting Information of our original theoretical paper [8].

$$\begin{aligned} \bar{v}_x &= \mu_{\mathrm{ep}} E \sin\varphi \\ \bar{v}_y &= (\mu_{\mathrm{EOF}} + \mu_{\mathrm{ep}}) E \cos\varphi + \bar{v}_{\mathrm{hd}} \end{aligned} \tag{3}$$

The hydrodynamic flow arises from a difference in pressure between the input and output. Below, a line above a symbol denotes its average value, calculated over all values of z. The average value of the resultant velocity, $\bar{v}$, of an introduced species is the sum of its electrophoretic velocity, the electroosmotic velocity, and the hydrodynamic velocity. The residence time depends on $\bar{v}_y$ (the y component of $\bar{v}$) and the lateral displacement is determined by $\bar{v}_x$:

$$\begin{aligned} R_S = 0.5 &\left| \frac{(\mu_{\mathrm{ep1}} - \mu_{\mathrm{ep2}}) L E \sin\varphi (\mu_{\mathrm{EOF}} E \cos\varphi + \bar{v}_{\mathrm{hd}})}{(\mu_{\mathrm{ap1}} E \cos\varphi + \bar{v}_{\mathrm{hd}})(\mu_{\mathrm{ap2}} E \cos\varphi + \bar{v}_{\mathrm{hd}})} \right| \\ &\times \left[\sqrt{\frac{w_0^2}{12} + \frac{2L}{\mu_{\mathrm{ap1}} E \cos\varphi + \bar{v}_{\mathrm{hd}}} \left[D_1 \left(1 + \left(\frac{\mu_{\mathrm{ep1}} E \sin\varphi}{\mu_{\mathrm{ap1}} E \cos\varphi + \bar{v}_{\mathrm{hd}}} \right)^2 \right) + \frac{h^2 E^2 \sin^2\varphi}{105 D_1} \left(\mu_{\mathrm{EOF}} + \frac{\mu_{\mathrm{ep1}} \bar{v}_{\mathrm{hd}}}{\mu_{\mathrm{ap1}} E \cos\varphi + \bar{v}_{\mathrm{hd}}} \right) \right.} \right. \\ &\quad \left. \times \left(\left(\mu_{\mathrm{EOF}} + \frac{\mu_{\mathrm{ep1}} \bar{v}_{\mathrm{hd}}}{\mu_{\mathrm{ap1}} E \cos\varphi + \bar{v}_{\mathrm{hd}}} \right) \left(\frac{1}{2} - \left(\frac{3\Lambda}{5} + \frac{\Gamma_1}{3} \right) \right) - \mu_{\mathrm{ep1}} P_1 \left(1 - \frac{\mu_{\mathrm{ep1}} E \cos\varphi}{\mu_{\mathrm{ap1}} E \cos\varphi + \bar{v}_{\mathrm{hd}}} \right) \right) \right] \\ &+ \left. \sqrt{\frac{w_0^2}{12} + \frac{2L}{\mu_{\mathrm{ap2}} E \cos\varphi + \bar{v}_{\mathrm{hd}}} \left[D_2 \left(1 + \left(\frac{\mu_{\mathrm{ep2}} E \sin\varphi}{\mu_{\mathrm{ap2}} E \cos\varphi + \bar{v}_{\mathrm{hd}}} \right)^2 \right) + \frac{h^2 E^2 \sin^2\varphi}{105 D_2} \left(\mu_{\mathrm{EOF}} + \frac{\mu_{\mathrm{ep2}} \bar{v}_{\mathrm{hd}}}{\mu_{\mathrm{ap2}} E \cos\varphi + \bar{v}_{\mathrm{hd}}} \right) \right.} \right. \\ &\quad \left. \times \left(\left(\mu_{\mathrm{EOF}} + \frac{\mu_{\mathrm{ep2}} \bar{v}_{\mathrm{hd}}}{\mu_{\mathrm{ap2}} E \cos\varphi + \bar{v}_{\mathrm{hd}}} \right) \left(\frac{1}{2} - \left(\frac{3\Lambda}{5} + \frac{\Gamma_2}{3} \right) \right) - \mu_{\mathrm{ep2}} P_2 \left(1 - \frac{\mu_{\mathrm{ep2}} E \cos\varphi}{\mu_{\mathrm{ap2}} E \cos\varphi + \bar{v}_{\mathrm{hd}}} \right) \right) \right] \right]^{-1} \end{aligned} \tag{4}$$

In μFFE, there are three major ways of manipulating the angles of deflection for particular species by: (i) adjusting the speed of the hydrodynamic flow, $\vec{v}_{hd}$, (ii) changing the electric field strength, or (iii) altering the angle between $\vec{E}$ and $\vec{v}_{hd}$. Our main approach will be to fix the hydrodynamic velocity and to vary E and φ.

When $\varphi > 90°$, increasing E has the effect of increasing $\bar{v}_x$ and decreasing $\bar{v}_y$ for positively charged species so that their lateral displacement increases. The electric field direction is chosen so that the species to be resolved have electrophoretic velocity components in the y direction, pointing against the hydrodynamic flow so that $\bar{v}_y < \bar{v}_{hd}$ (see Fig. 2). For cations, $90° < \varphi < 180°$, and for anions, $270° < \varphi < 360°$. As a result, the species to be separated move against the flow at different speeds and so spend unequal times in the separation channel. Species with larger electrophoretic velocities are delayed for longer and experience larger lateral displacements than species with smaller electrophoretic velocities. When the residence times of molecules increase, so do the widths of their streams but at a smaller rate than their lateral separation; overall resolution is improved.

$$R_s = 0.5\left|\frac{(\mu_{ep1}-\mu_{ep2})LE\sin\varphi(\mu_{EOF}E\cos\varphi+\bar{v}_{hd})}{(\mu_{ap1}E\cos\varphi+\bar{v}_{hd})(\mu_{ap2}E\cos\varphi+\bar{v}_{hd})}\right| \times\left[\sqrt{\frac{w_0{}^2}{12}+\frac{2D_1L}{\mu_{ap1}E\cos\varphi+\bar{v}_{hd}}+\frac{2D_1L\mu_{ep1}{}^2E^2\sin^2\varphi}{\left(\mu_{ap1}E\cos\varphi+\bar{v}_{hd}\right)^3}+\frac{Lh^2E^2\sin^2\varphi}{105D_1(\mu_{ap1}E\cos\phi+\bar{v}_{hd})}\left(\mu_{EOF}+\frac{\mu_{ep1}\bar{v}_{hd}}{\mu_{ap1}E\cos\phi+\bar{v}_{hd}}\right)^2}+\sqrt{\frac{w_0{}^2}{12}+\frac{2D_2L}{\mu_{ap2}E\cos\varphi+\bar{v}_{hd}}+\frac{2D_2L\mu_{ep2}{}^2E^2\sin^2\varphi}{\left(\mu_{ap2}E\cos\varphi+\bar{v}_{hd}\right)^3}+\frac{Lh^2E^2\sin^2\varphi}{105D_2(\mu_{ap2}E\cos\phi+\bar{v}_{hd})}\left(\mu_{EOF}+\frac{\mu_{ep2}\bar{v}_{hd}}{\mu_{ap2}E\cos\phi+\bar{v}_{hd}}\right)^2}\right]^{-1} \quad (7)$$

2.2. General theory of resolution in μFFE

If two analytes with charges of the same sign are continuously separated, the quality of their lateral separation can be characterized by their resolution, R_S (see Eq. (1)). Our general equation for resolution, is given by Eq. (4) (Eq. (4–20) in Ref. [8]). In Eq. (4), μ_{ap} is the apparent electrophoretic mobility equal to the sum of the electrophoretic mobility and the electroosmotic mobility.

In addition to addressing each of the assumptions discussed in the previous section, our general equation also takes into account the influences of temperature differences within the separation channel on viscosity, electrophoretic mobility, and diffusion coefficients. In this equation, the subscripts 1 and 2 refer to the two analytes, D refers to their diffusion coefficients, L and h are the length and height of the separating channel, w_0 is the width of the introduced sample stream, and the dimensionless parameters Λ, Γ, and P are the maximum fractional increases in the viscosity, diffusion coefficients, and electrophoretic mobilities, respectively, that result from temperature differences within the channel. The maximum temperature difference of the electrolyte in the channel is given by:

$$\Delta T_{max} = \frac{\kappa E^2 h^2}{8\lambda} \quad (5)$$

where κ is the electric conductivity of the electrolyte and λ is its thermal conductivity [9]. The definitions of Λ, Γ, and P are:

$$\Lambda = \frac{\alpha_\eta \kappa E^2 h^2}{8\lambda}, \quad \Gamma = \frac{\alpha_D \kappa E^2 h^2}{8\lambda}, \quad P = \frac{\alpha_\mu \kappa E^2 h^2}{8\lambda} \quad (6)$$

and α_η, α_D, and α_μ are the temperature coefficients of viscosity, diffusion, and electrophoretic mobility, respectively, each with values of approximately 0.02 K^{-1} [10–12].

It should be noted that Eq. (4) is a general equation that includes the influence of temperature differences in the z direction. Under normal operating conditions ($h \leq 100\,\mu m$, $E \leq 300\,V\,cm^{-1}$, and $\kappa \leq 0.05\,S\,m^{-1}$, $\Delta T < 0.1\,K$), these temperature effects can be ignored. In such cases, a simplified form of our general equation can be used to determine resolution. Eq. (7) is a deconvoluted form of Eq. (4) from Ref. [5] and is derived in Supplementary Content.

Inspection of Eqs. (4)–(7) shows that apart from its dependence on the angle φ between the electric field and the hydrodynamic flow, resolution can be altered through adjusting: (i) the conductivity of the buffer, (ii) the strength of the electric field, (iii) the average velocity of the hydrodynamic flow, (iv) the height of the separation channel, and (v) the size and sign of the electroosmotic mobility. We will consider these influences on resolution one at a time in conjunction with φ for two groups of analytes.

For illustration, we chose two pairs of species: (i) two single strands of DNA with 75 and 76 base pairs as an example of large negatively charged molecules with relatively small diffusion coefficients and (ii) Mg^{2+}(aq) and Mn^{2+}(aq) as an example of small positively charged molecules with relatively large diffusion coefficients. Each pair was chosen so that the difference in electrophoretic mobility of the two molecules was about 1% of their average electrophoretic mobility. The values of μ_{ep} and D for the single strands of DNA ($\mu_{ep1} = -1.813 \times 10^{-8}$ and $\mu_{ep2} = -1.830 \times 10^{-8}\,m^2\,s^{-1}\,V^{-1}$, $D_1 = 4.99 \times 10^{-11}$ and $D_2 = 5.04 \times 10^{-11}\,m^2\,s^{-1}$) were calculated using the data from Nkodo et al. [13] and the data for Mg^{2+}(aq) and Mn^{2+}(aq) came from tabulated values of Vanysek [14] ($\mu_{ep1} = 5.493 \times 10^{-8}$ and $\mu_{ep2} = 5.542 \times 10^{-8}\,m^2\,s^{-1}\,V^{-1}$, $D_1 = 7.06 \times 10^{-10}$ and $D_2 = 7.12 \times 10^{-10}\,m^2\,s^{-1}$).

2.3. The effect of electrolyte conductivity on resolution

The conductivity of the electrolyte affects resolution *via* Joule heating (see Eq. (5)), which may exacerbate dispersion by introducing convective transfer of charged species due to buoyancy effects if channel heights are sufficiently large [7]. As the temperature difference within the channel is directly proportional to the conductivity; a low-conductivity electrolyte is obviously preferable to minimize these undesirable effects. The maximum conductivity that can be used varies inversely with h^2E^2; thinner channels allow for stronger electric fields and/or higher conductivity electrolytes. A close examination of Eq. (4) shows that only hydrodynamic dispersion is influenced by these temperature effects. Practitioners may also need to take into account changes to the electroosmotic flow as a consequence of varying the ionic strength of the electrolyte [15].

2.4. The influence of electric field strength on resolution

To maximize the space available in the x direction for the separation, it is expedient that the sample always enters at the same location (at a small x value) and that charged species be they anions or cations are deflected in the same direction. To facilitate this, angles of $90° < \varphi < 180°$ are used for cations and $270° < \varphi < 360°$

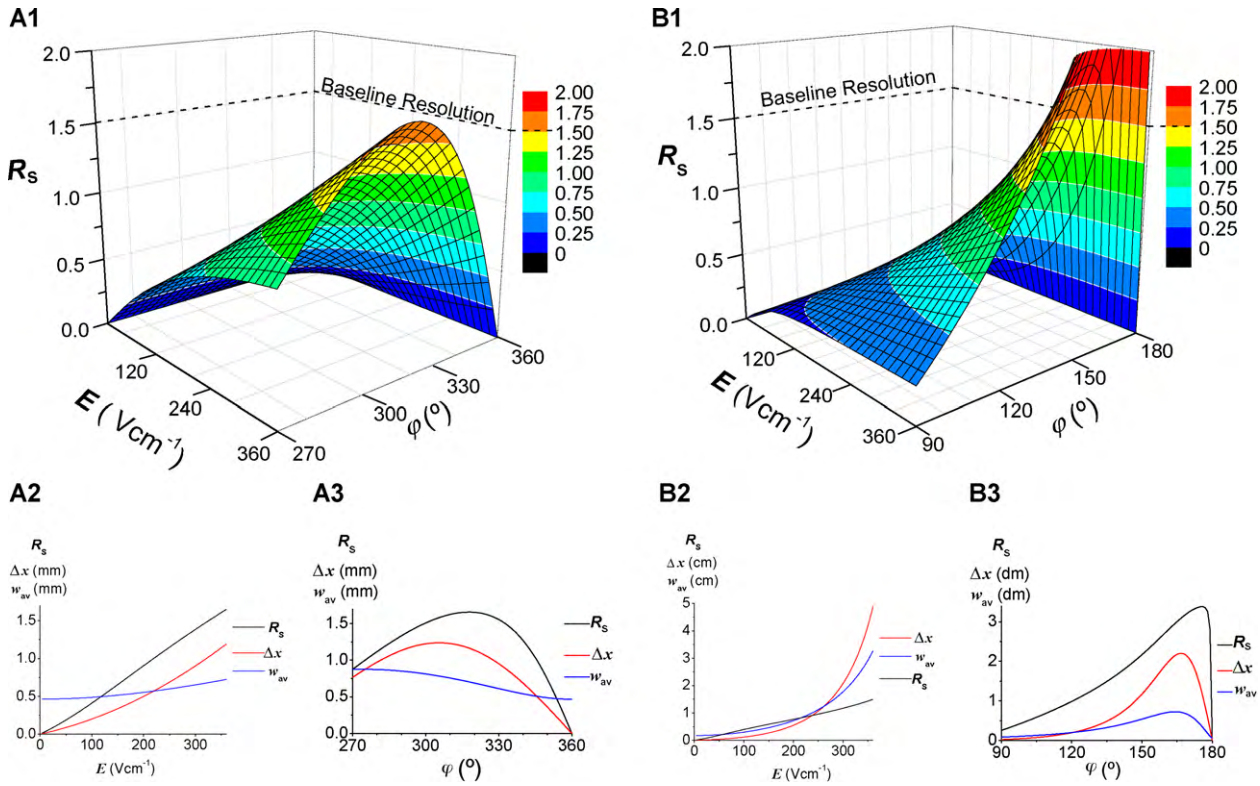

Fig. 3. The variation of resolution, R_S, with electric field strength, E, and the angle, φ, between the electric field and the hydrodynamic flow, for: two large molecules (A) and two small molecules (B). The conditions used in all panels were: $\bar{v}_{hd} = 0.4$ mm s^{-1}, $h = 20$ μm, and $\kappa = 0.043$ S m^{-1}. In (A1–A3), $\mu_{EOF} = 1.80 \times 10^{-8}$ m^2 s^{-1} V^{-1}, and in (B1–B3), $\mu_{EOF} = -4.50 \times 10^{-8}$ m^2 s^{-1} V^{-1}. The vertical scale in B1 has been truncated for clarity of presentation. Panels (A2 and B2) depict the variation of resolution, separation, and average bandwidth with electric field strength for fixed φ values of 315° and 135°, respectively. Panels (A3 and B3) show the variation of resolution, separation, and average stream width with φ for $E = 360$ V cm^{-1}.

for anions. Fig. 3 illustrates the dependence of resolution on electric field strength and the angle between the field vector and the hydrodynamic flow. The plots were generated using conditions that minimize hydrodynamic dispersion for each of the analyte types. The wall chemistry of the substrates need to be matched to the species being separated so that $\mu_{EOF} \approx -\mu_{ep}$ [3,7] Appropriate wall coatings would be required to achieve this i.e. cationic surfactants/polymers for positively charged analytes and anionic surfactants/polymers for negatively charged species [16,17].

Baseline resolution is characterized by values: $R_S \geq 1.50$ [6]; the orange and red surfaces of the plots show conditions for which baseline resolution of the separated species would occur. (For interpretation of the references to color in text, the reader is referred to the web version of the article)

Both panels A1 and B1 of Fig. 3 show an improvement in resolution with increasing E for all values of φ. This occurs since lateral separation, Δx, grows quicker than the average width of the separated streams, w_{av}, with increasing E (panels 3A2 and 3B2 in Fig. 3). Further increases in E, would eventually result in one or both species having v_y (the y-projection of the resultant velocity) in the opposite direction to the hydrodynamic flow so that collection of both species would no longer be possible. Collection of both species is possible if $\varphi < \varphi_{max}$, where φ_{max} is the angle that makes $\bar{v}_y = 0$, for the component with the larger electrophoretic mobility. φ_{max} can be found by rearranging Eq. (3) to:

$$\varphi_{max} = \pm \arccos \frac{-\bar{v}_{hd}}{(\mu_{EOF} + \mu_{ep})E} \tag{8}$$

In Eq. (8), the sign of the angle depends on one of the two mirror-symmetry cases.

For a fixed value of E, the influence of φ on resolution is not straightforward but depends on the nature of the species to be separated and their velocity components parallel to the hydrodynamic flow. For the slowly diffusing large molecules with $\bar{v}_y \simeq \bar{v}_{hd}$, the widths of the separated streams generally decrease as φ increases, but the lateral separation reaches a maximum at an intermediate value of φ leading to an overall improvement in resolution (see Fig. 3A3). The decrease in w_{av} with increasing φ is a result of the strong dependences on $\sin^2\varphi$ for (i) diffusion in the y direction and (ii) hydrodynamic dispersion (see Eq. (7)). Due to the large hydrodynamic velocity (relative to the net electrophoretic velocity) φ has little influence on the species' residence time. The slight increase in variance associated with diffusion in the x direction is more than compensated for by decreases in diffusion in the y direction and in hydrodynamic dispersion.

Modeling for the small ions suggests that great improvements in resolution can be achieved using non-orthogonal μFFE. Reasons for this are: (i) the smaller influence on resolution of hydrodynamic dispersion and (ii) the greater difference in molecules' residence times when $\bar{v}_y \ll \bar{v}_{hd}$ (notice the larger scale for Δx and w_{av} in Fig. 3B2 and B3). The construction of suitable devices to accommodate these separations will be challenging from an engineering point of view using traditional photolithography methods due to the requirement of very large aspect ratios ($w/h \sim 40\,000$ in Fig. 3B3). Alternative fabrication methods may need to be considered such as the use of a high precision milling machine to create the separation channel or the use of a spacer between two optically-smooth surfaces [18–20].

It should be recognized that using the conditions shown, it is not possible for orthogonal μFFE to achieve baseline resolution for either group of analytes even at the maximum field strength of

$3.6 \times 10^4\,\mathrm{V\,m^{-1}}$ due to similarities of the electrophoretic mobilities of the species. Fig. 3A1 shows that baseline resolution is possible for the DNA fragments at a minimum field strength of $E = 3.3 \times 10^4\,\mathrm{V\,m^{-1}}$ if $\varphi = 316°$. At the maximum field strength, $E = 3.6 \times 10^4\,\mathrm{V\,m^{-1}}$, the resolution increases from 0.88 to 1.66 when φ increases from 270° to 318°. Similarly, Fig. 3B1 shows that by adjusting φ, the small ions can be baseline resolved if $E \geq 3.4 \times 10^4\,\mathrm{V\,m^{-1}}$ and $157° \leq \varphi \leq 165°$. The gain in resolution is more noticeable for the small ions when the maximum field strength is used; using φ in the desired range, R_S can be increased by more than one order of magnitude (from 0.26 to 3.37). These dramatic improvements in resolution are not restricted to small ions. If, for example, the hydrodynamic flow velocity is reduced during the separation of the large molecules, the same improvements in resolution are possible but at the expense of sample throughput and the need for very wide channels.

As a rule of thumb, the maximum resolution can be achieved when $\bar{v}_y$ is much smaller than $\bar{v}_{hd}$ but still greater than zero. Under these conditions, resolution is very sensitive to slight variations in φ or E. The solution to this sensitivity is any one of the following: (i) reduction of the electric field strength, (ii) increase in the hydrodynamic velocity, or (iii) making μ_{EOF} larger in magnitude but opposite in sign to μ_{ep}.

To summarize the influence of electric field strength on resolution (provided that $\Delta T < 1\,°C$ so that convection effects are avoided [7], and $\bar{v}_y > 0$ so that both species can be collected), resolution is always improved by increasing the field strength; however, the extent of the improvement is analyte dependent. Our computer modeling showed that above a threshold electric field strength, resolution increases linearly with E for orthogonal μFFE, which is in agreement with previously published results [21]. For non-orthogonal μFFE, the relationship between R_S and E was linear for the large molecules but became increasingly non-linear for small molecules as φ increased. The R_S vs. E dependencies for small molecules are well described by $R_S = kE^n$ $(1 < n < 2)$. The resolution for a particular field strength can be maximized by adjusting φ so that $\bar{v}_y \ll \bar{v}_{hd}$ and $\bar{v}_y > 0$ for the species with the greater value of μ_{ep}.

2.5. The effect of hydrodynamic velocity on resolution

Eq. (1) shows that resolution depends on the lateral separation Δx and the widths of the separated streams, w. The lateral separation of two species is equal to the numerator of Eqs. (4) and (7):

$$\Delta x = \left| \frac{(\mu_{ep1} - \mu_{ep2})LE \sin\varphi(\mu_{EOF}E\cos\varphi + \bar{v}_{hd})}{(\mu_{ap1}E\cos\varphi + \bar{v}_{hd})(\mu_{ap2}E\cos\varphi + \bar{v}_{hd})} \right| \tag{9}$$

Eq. (9) is derived from first principles in Supplementary Content; it is more complicated than the expression used by Fonslow and Bowser [21], as in non-orthogonal μFFE, the species spend unequal times in the electric field. In general, the lateral separation is inversely proportional to the average hydrodynamic velocity as the faster the velocity, the shorter the residence time.

The width of a separated stream depends on the total variance as shown below [6,22]:

$$w = 4\sqrt{\sigma_{tot}^2} \tag{10}$$

where σ_{tot}^2 is total variance which has contributions from four main sources: sample introduction, diffusion in the x direction, diffusion in the y direction, and hydrodynamic dispersion. In the absence of excessive Joule heating or a change to the absorption of species to the walls, these four sources of dispersion can be calculated using Eq. (11), which differs from previous equations by taking into account diffusion in the direction of the hydrodynamic flow and the influence of the non-orthogonal electric field [3,4,19–22].

$$\sigma_{tot}^2 = \frac{w_0^2}{12} + \frac{2DL}{\mu_{ap}E\cos\varphi + \bar{v}_{hd}} + \frac{2DL\mu_{ep}{}^2E^2\sin^2\varphi}{(\mu_{ap}E\cos\varphi + \bar{v}_{hd})^3} + \frac{h^2LE^2\sin^2\varphi}{105D\mu_{ap}E\cos\varphi + \bar{v}_{hd}}\left(\mu_{EOF} + \frac{\bar{v}_{hd}\mu_{ep}}{\mu_{ap}E\cos\varphi + \bar{v}_{hd}}\right)^2 \tag{11}$$

Eq. (11) illustrates that the variance associated with sample introduction is independent of the hydrodynamic flow and depends only on the width of the introduced sample stream [22]. The influence of diffusion in the x and y directions depends on the hydrodynamic velocity to the powers of −1 and −3, respectively [5,21–24]. The variance associated with hydrodynamic dispersion depends on $D^{-1}\bar{v}_{hd}^{-1}$, so that it has a major impact for molecules with small diffusion coefficients [21].

Plots of the variation of resolution with the average hydrodynamic velocity are shown for both large and small molecules in Fig. 4. For the large molecules and conditions similar to those described in Fig. 3A, but with E fixed at $3.6 \times 10^4\,\mathrm{V\,m^{-1}}$, resolution is favored using lower velocities which increase the residence times. Using the conditions described, baseline resolution is possible for velocities in the range: $0.10 \leq \bar{v}_{hd} < 0.49\ \mathrm{mm\ s^{-1}}$. For the small molecules, baseline separation is possible over a similar range of hydrodynamic velocities ($0.10 \leq \bar{v}_{hd} < 0.37\ \mathrm{mm\ s^{-1}}$).

Discontinuities in R_S vs. $\bar{v}_{hd}$ occur when $\varphi > \varphi_{max}$ since under these conditions both species cannot be collected at the output. Using conditions similar to those described in Fig. 3B3, but with $E = 3.6 \times 10^4\,\mathrm{V\,m^{-1}}$, and a more negative value of μ_{EOF}, an improvement in separating power of more than 11 times over orthogonal μFFE is observed.

For small molecules, it is possible, to extend the range of velocities that enable baseline resolution, and thus increase the rate at which a sample stream can be separated by manipulating the electroosmotic mobility. This concept is illustrated and discussed in more detail in (Supplementary Content and Fig. S1).

In summary, resolution generally increases with residence time (decreasing hydrodynamic velocity), however if $\bar{v}_{hd}$ is too small, diffusion becomes excessive and/or collection of both species is no longer possible. The value of φ for maximum resolution increases with the hydrodynamic velocity.

2.6. The role of electroosmotic flow in resolution

Examination of Eq. (11) shows that there are two mechanisms by which varying the electroosmotic flow can affect resolution. The first mechanism is well known in macro FFE to resolve large molecules; the total variance can be decreased if the electroosmotic mobility is opposite in sign and magnitude to the electrophoretic mobility of the slower of species to be separated [4,7,8]:

$$\mu_{EOF} \simeq -\mu_{ep1},\ \left|\mu_{EOF}\right| < \left|\mu_{ep1}\right| < \left|\mu_{ep2}\right| \tag{12}$$

By this means, the recirculating electroosmotic flow compensates for velocity differences in the y–z plane; indeed, Eq. (11) predicts that hydrodynamic dispersion should reduce to ~0 for the slower species [4].

The second mechanism, by which varying μ_{EOF} affects resolution, is through its influence on $\bar{v}_y$ (see Eq. (3)). The dramatic improvement in resolution, that can be achieved using non-orthogonal μFFE, comes from the separating species having different residence times, t_i.

$$t_i = \frac{L}{\bar{v}_{y,i}} = \frac{L}{(\mu_{EOF} + \mu_{ep,i})E\cos\varphi + \bar{v}_{hd}}, \quad i = 1, 2 \tag{13}$$

Note, that the species with the larger electrophoretic mobility has a greater residence time and is displaced further in the x

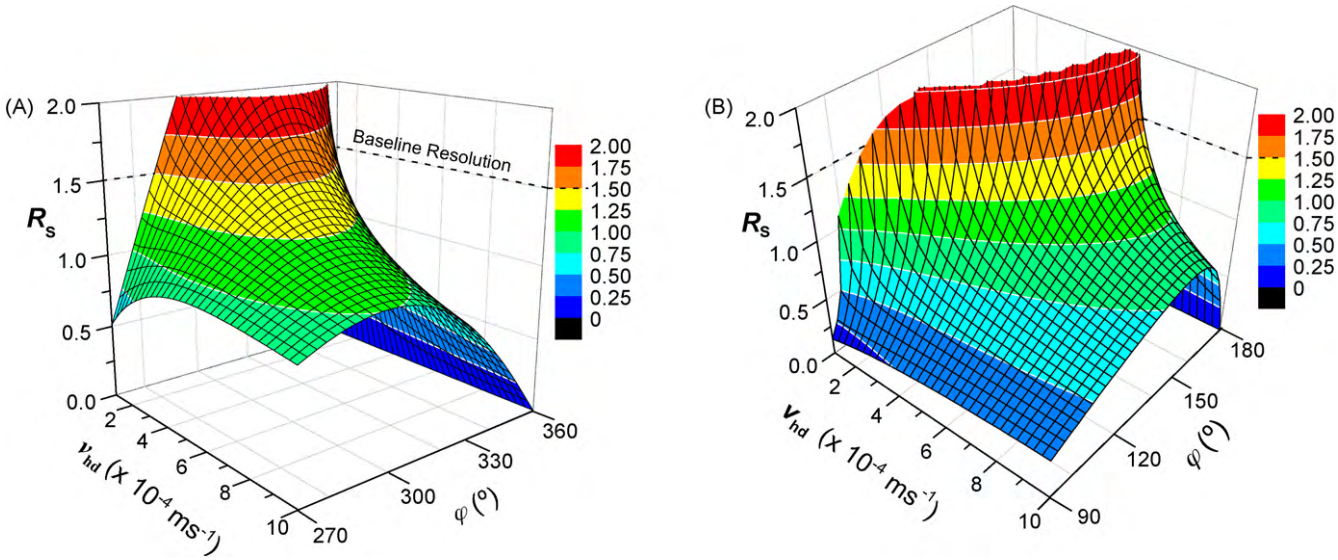

Fig. 4. The variation of resolution with hydrodynamic velocity and the angle that it makes with the electrical field for two large molecules (A) and two small molecules (B). The conditions were: $h = 20\,\mu m$, $E = 3.6 \times 10^4\,V\,m^{-1}$, $L = 0.050\,m$, while varying the average hydrodynamic velocity from 0.1 to 1.0 mm s^{-1}. In (A) $\mu_{ep1} = -1.813 \times 10^{-8}$, $\mu_{ep2} = -1.832 \times 10^{-8}$, and $\mu_{EOF} = 1.80 \times 10^{-8}\,m^2\,s^{-1}\,V^{-1}$ and in (B) $\mu_{ep1} = 5.493 \times 10^{-8}$, $\mu_{ep2} = 5.542 \times 10^{-8}$, and $\mu_{EOF} = -5.28 \times 10^{-8}\,m^2\,s^{-1}\,V^{-1}$. The dashed line in each panel represents baseline resolution.

direction than the species with the lower electrophoretic mobility. When $v_{y,i} \approx 0$, a small change in μ_{EOF} can have a major impact on t_i and, therefore, on the displacement in the x direction. However, decreasing $\bar{v}_y$ by changing μ_{EOF} will not necessarily lead to improved resolution. For large molecules, a deviation from the strategy of Eq. (12) leads to increased hydrodynamic dispersion and decreased resolution. For small molecules, the effects of μ_{EOF} on hydrodynamic dispersion are less significant so that adjustment of the electroosmotic flow may be useful for tuning the separation to a particular hydrodynamic flow rate. Plots of R_S vs. μ_{EOF} and φ for large and small molecules can be found in Fig. S2 of the Supplementary Content.

2.7. The effect of channel height on resolution

Varying the channel height has significant effects on the rate at which a sample stream is separated, Joule heating, and hydrodynamic dispersion. Sample throughput and heat production increase linearly with h but the temperature difference (in the z direction) and hydrodynamic dispersion both increase with h^2. Reducing h is particularly important for biological species which denature at elevated temperatures and for separating species that have relatively small diffusion coefficients. Fig. 5A shows the variation of resolution for the large molecules as a function of channel height and φ. As the channel height increases, there is a monotonous decrease in resolution. Baseline resolution of these species is not possible for orthogonal μFFE using the conditions described. Non-orthogonal μFFE under the same conditions improves resolution for all channel heights and baseline resolution is possible for $h \leq 50\,\mu m$ if $\varphi = 318°$. Fig. 5B shows the corresponding plot for small ions; under these conditions, orthogonal μFFE is unable to resolve these species either. Baseline resolution is possible for all of the channel heights in the range 10–100 μm using non-orthogonal μFFE if $\varphi = 135°$. The sudden decline in resolution for $\varphi > 135°$ occurs because $\varphi > \varphi_{max}$.

2.8. The limiting difference in electrophoretic mobility that can be baseline resolved

By rearranging Eq. (7), it is possible to find an expression for $\Delta\mu_{ep\,lim}$, the minimum difference in electrophoretic mobility of species that can be baseline resolved. According to convention, baseline resolution requires $R_S \geq 1.50$ [6]. If we assume that: (i) Joule heating effects are insignificant, (ii) electrophoretic mobilities are similar with an average value, μ, and (iii) diffusion coefficients can be represented by an average value, D, and set the value of R_S to 1.50, then Eq. (14) is a general expression for finding $\Delta\mu_{ep\,lim}$:

$$\Delta\mu_{ep\,lim} = \sqrt{\frac{3w^2\left\{(\mu_{EOF}+\mu_{ep})E\cos\varphi+\bar{v}_{hd}\right\}^4}{L^2E^2\sin^2\varphi(\mu_{EOF}E\cos\varphi+\bar{v}_{hd})^2} + \frac{72D\left\{(\mu_{EOF}+\mu_{ep})E\cos\varphi+\bar{v}_{hd}\right\}^3}{LE^2\sin^2\varphi(\mu_{EOF}E\cos\varphi+\bar{v}_{hd})^2} + \frac{72D\mu_{ep}^2\left\{(\mu_{EOF}+\mu_{ep})E\cos\varphi+\bar{v}_{hd}\right\}}{L(\mu_{EOF}E\cos\varphi+\bar{v}_{hd})^2} + \frac{72h^2\left\{(\mu_{EOF}+\mu_{ep})E\cos\varphi+v_{hd}\right\}^3}{210DL(\mu_{EOF}E\cos\varphi+\bar{v}_{hd})^2}\left(\mu_{EOF}+\frac{\mu_{ep}v_{hd}}{(\mu_{EOF}+\mu_{ep})E\cos\varphi+v_{hd}}\right)^2} \quad (14)$$

Analysis of Eq. (14) demonstrates a reduction in $\Delta\mu_{ep\,lim}$ when using non-orthogonal FFE compared to orthogonal FFE. Indeed, if the electrophoretic velocity has a component opposite to the direction of the hydrodynamic flow, then the following inequality will be satisfied:

$$v_y = \bar{v}_{hd} + (\mu_{EOF} + \mu_{ep})E\cos\varphi < \bar{v}_{hd} \quad (15)$$

It follows that each of the terms that contribute to $\Delta\mu_{ep\,lim}$ in orthogonal μFFE, can be decreased in non-orthogonal μFFE. The greatest improvements can be obtained when $v_y \to 0$ but remains positive. To illustrate the superior resolving power of non-orthogonal μFFE, it is instructive to consider what minimum difference in electrophoretic mobility can be resolved

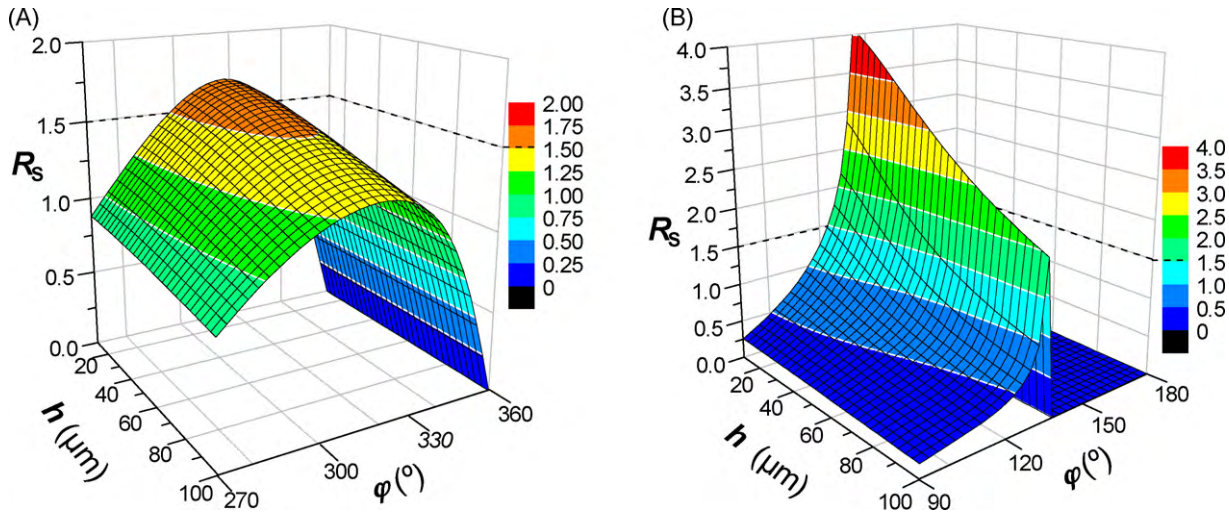

Fig. 5. Variation of resolution with channel height for: two large molecules (A) and two small molecules (B). The conditions used were identical to those of Fig. 3 except that the electric field strength was fixed, $E = 3.6 \times 10^4\ \mathrm{V\,m^{-1}}$, and the channel height was varied from 10 to 100 μm. The onset of baseline resolution is shown by $R_S = 1.5$.

using orthogonal and non-orthogonal μFFE with reference to the examples above. Plots for the minimum difference in resolution ($\Delta\mu_{\mathrm{ep\,lim}}$) vs. E and φ are illustrated in Fig. S3 of the Supplementary Content. Not surprisingly, the smallest difference in electrophoretic mobility that can be resolved occurs for conditions which give the best resolution and for conditions in which Joule heating is not problematic, increasing the electric field strength reduces the size of $\Delta\mu_{\mathrm{ep\,lim}}$. For the conditions used in Fig. 3A, $\Delta\mu_{\mathrm{ep\,lim}} = 2.90 \times 10^{-10}\ \mathrm{m^2\,s^{-1}\,V^{-1}}$ for orthogonal μFFE, but decreased to $1.54 \times 10^{-10}\ \mathrm{m^2\,s^{-1}\,V^{-1}}$ by increasing φ to 318°; i.e. $\Delta\mu_{\mathrm{ep\,lim}} < 1\%$ of μ_{ep}. Further improvements can be made by reducing the hydrodynamic flow so that $v_y \rightarrow 0$ but is still positive. For example, by reducing $\bar{v}_{\mathrm{hd}}$ to $5 \times 10^{-5}\ \mathrm{m\,s^{-1}}$, $\Delta\mu_{\mathrm{ep\,lim}}$ can be made less than $5 \times 10^{-11}\ \mathrm{m^2\,s^{-1}\,V^{-1}}$ or less than 0.3% of μ_{ep}; however this would reduce the throughput by a factor of 8 and would require an exceedingly wide separation channel.

Using numerical methods, we have demonstrated that non-orthogonal μFFE has the potential to offer greatly improved resolution compared to conventional μFFE; however, it should be stressed that practical issues such as creating a non-orthogonal electric field need to be considered to realize these improvements.

2.9. Creating a non-orthogonal electric field

In this section, we will discuss the four potential device designs that are illustrated in Fig. 6A–D. For each of the designs, an in-house Pascal program (Laplace.dll), which can be downloaded from the research section of the site: http://www.chem.yorku.ca/profs/krylov/ was used to simulate the shape of electric field. For each of the diagrams, the direction of the electric field is indicated by the curved or straight lines which go from the positive electrode (shown in red) to the negative one (blue).

The simplest design, shown in Fig. 6A, has two short staggered electrodes on opposite sides of the separation channel. Although such a design may be used to illustrate the proof of principle for non-orthogonal μFFE and is likely to have fewer problems with removal of bubbles formed at the electrodes, the non-uniform nature of the field would lead to poor reproducibility and increased dispersion.

Fig. 6B shows a relatively simple design featuring parallel electrodes at an angle to the separation channel (shown in lilac), and positioned outside the separation channel but still in contact with the electrolyte, so that the region containing electrolyte must be extended beyond the separation channel. The advantage of this design is that it would produce a uniform electric field within the

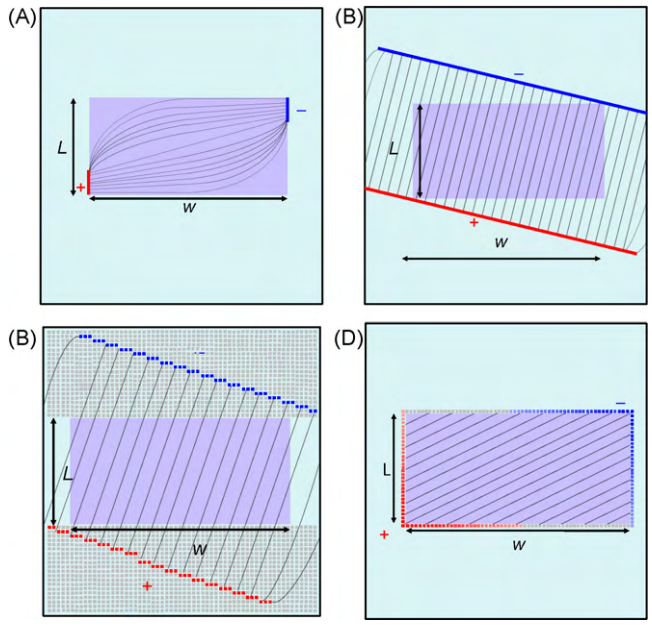

Fig. 6. Schematic FFE designs showing variation of E with design. In each panel, the aqua colored area represents a chamber which is in contact with the buffered electrolyte. The lilac areas show the separation channels which have a length of L and a width of W. Samples are introduced at the top left hand corner of the separation channel and separated analytes are collected along the bottom of the separation channel. Angled lines represent the direction of the electric field from + to −. Positive electrodes are shown in red and negative electrodes in blue. Staggered small solid electrodes produce a non-uniform electric field (A). Fixed external angled electrodes produce a uniform electric field in the separation channel with a fixed angle (B). Arrays of individually switched microelectrodes (depicted as small squares) external to the separation channel can be used to produce a uniform electric field of variable direction; gray squares show microelectrodes for which the voltage is floating (C). A single array of individually controlled microelectrodes surrounding the separation channel produces the desired electric field; the gradation of color represents the variation in magnitude of the voltage applied to each microelectrode (D). (For interpretation of the references to color in text, the reader is referred to the web version of the article.)

separation channel. A limitation of such a system is that the angle of the electric field would be fixed so that there would be no means of adjusting φ after fabrication of the device. However, resolution could still be maximized by adjusting the electric field strength and/or the hydrodynamic flow rate to match the chosen value of φ.

Fig. 6C shows a more complex but versatile design in which two large arrays of microelectrodes could be individually switched on or off in the device to produce a uniform electric field. This design would have the facility to produce large values of φ. The small squares represent the locations of microelectrodes; these would be of a size small enough and separated sufficiently so as to cause minimal disruption to the laminar hydrodynamic flow. On the grids, positions marked in red indicate electrodes with a positive potential and those marked in blue a negative potential while those marked in gray would have their potential floating. Each of the electrodes marked by a particular color (red or blue) would have the same electric potential, enabling a single power supply to be used to control the device. The resulting electric field would be similar to that of the device in Fig. 6B but this design would offer greater flexibility in controlling the direction of the electric field; a range of values of φ would be possible.

Fig. 6D illustrates a design that would be most difficult to engineer but which potentially offers the greatest versatility. It consists of an array of microelectrodes on the perimeter of the separation channel attached to individual high voltage power supplies. By controlling the voltage of each of the individual electrodes, it is possible to vary φ continuously making it suitable for the separation of cations or anions with very similar electrophoretic mobilities. The program (Laplace.dll) allows the user to input values of φ and calculates the relative voltages that are required for each of the microelectrodes surrounding the separation channel. Obviously the electronics needed to control such a system would need to be far more complicated than for the previous designs and the cost of building such an instrument would be at least an order of magnitude more expensive.

3. Conclusions

Our modeling demonstrates that for any experimental conditions, resolution can be improved using a non-orthogonal electric field rather than the orthogonal geometry that has been used exclusively in the past; the improvement can be as much as an order of magnitude. Using our equation for resolution, we derived a useful equation to determine the minimum difference in electrophoretic mobility, $\Delta\mu_{\mathrm{ep\,lim}}$ for species that can be baseline resolved by non-orthogonal μFFE. This new equation corroborates the superior separating power of non-orthogonal μFFE over orthogonal μFFE under the same conditions as a result of its ability to confer different residence times to species differing only slightly in electrophoretic mobility. Under ideal conditions, $\Delta\mu_{\mathrm{ep\,lim}} < 0.5\%\mu_{\mathrm{ep}}$, making it ideal for resolving difficult-to-separate species.

Provided that both species to be separated have resultant velocities with positive components in the direction of the hydrodynamic flow, and Joule heating is not excessive, resolution increases with electric field strength.

Hydrodynamic velocity has a significant impact on resolution. At very slow hydrodynamic velocities, diffusion limits resolution [23]. At relatively fast flow rates, lateral separation is limited by short residence times and non-orthogonal μFFE offers only marginal improvements. In general, the greatest improvements in resolution can be achieved when the electrophoretic velocity and the speed of the hydrodynamic flow are similar in size. In such cases resolution can be maximized by adjusting φ so that $\vec{v}_y \rightarrow 0$ for the species with the larger electrophoretic mobility.

When hydrodynamic dispersion is significant, considerable gains in resolution can be obtained by adjusting the electroosmotic mobility so that it has the opposite sign and same magnitude as the slower of the species to be separated. Alternatively, as is the case for small molecules, when hydrodynamic dispersion is less critical, the electroosmotic flow can be suppressed to facilitate higher flow rates without adversely affecting resolution.

The choice of channel height has profound effects on Joule heating, hydrodynamic dispersion and throughput. Resolution always improves by decreasing the height of the separation channel but to the detriment of sample throughput. Our model enables *ab initio* calculations to be made of the desired channel height for a particular pair of species before investing considerable resources into building a suitable apparatus.

Our theoretical work should stimulate the practical realization of non-orthogonal μFFE and will stimulate further development of FFE and serve as a tool for the design of efficient practical FFE devices.

Acknowledgement

Funding was generously provided by the Natural Sciences and Engineering Research Council of Canada.

Appendix A. Supplementary data

Supplementary data associated with this article can be found, in the online version, at doi:10.1016/j.aca.2010.06.002.

References

[1] C.C. Wiles, P. Watts, Eur. J. Org. Chem. 10 (2008) 1655–1671.
[2] K. Geyer, J.D.C. Codee, P.H. Seeberger, Chem. Eur. J. 12 (2006) 8434–8442.
[3] N. Pamme, Lab Chip 7 (2007) 1644–1659.
[4] K. Hannig, in: Th. Gerritsen (Ed.), Modern Separation Methods of Macromolecules and Particles, John Wiley and Sons, New York, 1969, pp. 45–69.
[5] V. Okhonin, C.J. Evenhuis, S.N. Krylov, Anal. Chem. 82 (2010) 1183–1185.
[6] D.C. Harris, Quantitative Chemical Analysis, 4th ed., W.H Freeman and Company, New York, 1995.
[7] A. Strickler, T. Sacks, Ann. N.Y. Acad. Sci. 209 (1973) 497–514.
[8] V. Okhonin, C.J. Evenhuis, S.N. Krylov, Anal. Chem. 82 (2010) 1183–1185 (Supporting Information).
[9] E. Ravoo, P.J. Gellings, T. Vermeulen, Anal. Chim. Acta 38 (1967) 219–232.
[10] R.C. Weast (Ed.), National Bureau of Standards in Handbook of Chemistry and Physics, 58th ed., CRC Press, Cleveland, 1977, p. F51.
[11] A.C.F. Ribeiro, O. Ortona, S.M.N. Simoes, C.A.V. Santos, P.M.R.A. Prazeres, A.J.M. Valente, V.M.M. Lobo, H.D. Burrows, J. Chem. Eng. Data 51 (2006) 1836–1840.
[12] C.J. Evenhuis, V. Hruska, R.M. Guijt, M. Macka, B. Gas, P.J. Marriott, P.R. Haddad, Electrophoresis 28 (2007) 3759–3766.
[13] A.E. Nkodo, J.M. Garnier, B. Tinland, H. Ren, C. Desruisseaux, L.C. McCormick, G. Drouin, G.W. Slater, Electrophoresis 22 (2001) 2424–2432.
[14] P. Vanysek, in: D.R. Lide (Ed.), CRC Handbook of Chemistry and Physics, 89th ed., CRC Press/Taylor and Francis, Boca Raton, 2009, p5–76 (Internet edition).
[15] B.J. Kirby, E.F.J. Hasselbrink, Electrophoresis 25 (2004) 187–202.
[16] C.A. Currie, J.S. Shim, S.H. Lee, C. Ahn, P.A. Limbach, H.B. Halsall, W.R. Heineman, Electrophoresis 30 (2009) 4245–4250.
[17] J.E. Melanson, N.E. Baryla, C.A. Lucy, Trends Anal. Chem. 20 (2001) 365–374.
[18] E. Rodrigues, R.A.S. Lapa, Microchim. Acta 166 (2009) 189–195.
[19] E. Rodrigues, R.A.S. Lapa, Anal. Sci. 25 (2009) 443–448.
[20] A. Chartogne, U.R. Tjaden, J. Van der Greef, Rapid Commun. Mass Spectrom. 14 (2000) 1269–1274.
[21] B.R. Fonslow, M.T. Bowser, Anal. Chem. 78 (2006) 8236–8244.
[22] D.E. Raymond, A. Manz, H.M. Widmer, Anal. Chem. 68 (1996) 2515–2522.
[23] D. Kohlheyer, J.C.T. Eijkel, A. van den Berg, R.B.M. Schasfoort, Electrophoresis 29 (2008) 977–993.
[24] R.T. Turgeon, M.T. Bowser, Anal. Bioanal. Chem. 394 (2009) 187–198.

Supplementary Content

Non-Orthogonal Micro-Free Flow Electrophoresis: from Theory to Design Concept

Christopher J. Evenhuis, Victor Okhonin, and Sergey N. Krylov*

Department of Chemistry and Centre for Research on Biomolecular Interactions, York University, Toronto, Ontario M3J 1P3, Canada

Table of Contents

Page number

1. Derivation of Equation 7 in the main text……... S-2

2. Derivation of Equation 9 in the main text…… S-3

3. Factors affecting resolution in non-orthogonal μFFE……. S-3

   3.1 Resolution of small molecules at an elevated hydrodynamic flow rate…… S-4

   3.2. Plots of the variation of resolution with electroosmotic mobility for large and small molecules ……. S-5

4. The minimum difference in electrophoretic mobility that can be baseline resolved, $\mu_{ep\ lim}$……. S-6

   4.1. Derivation of a general equation for the minimum difference in electrophoretic mobility that can be baseline resolved, $\mu_{ep\ lim}$……... S-6

   4.2 Plots of the variation of $\Delta\mu_{ep\ lim}$ *vs* E for large and small molecules……... S-8

1. Derivation of Equation 7 in main manuscript

$$R_S = \frac{\left|\dfrac{\left(\mu_{\mathrm{ep1}}-\mu_{\mathrm{ep2}}\right)LE\sin\varphi\left(\mu_{\mathrm{EOF}}E\cos\varphi+\bar{v}_{\mathrm{hd}}\right)}{\left(\mu_{\mathrm{ap1}}E\cos\varphi+\bar{v}_{\mathrm{hd}}\right)\left(\mu_{\mathrm{ap2}}E\cos\varphi+\bar{v}_{\mathrm{hd}}\right)}\right|}{2\left(\sqrt{\dfrac{w_0^{\,2}}{12}+\dfrac{2L}{\mu_{\mathrm{ap1}}E\cos\varphi+\bar{v}_{\mathrm{hd}}}\left(D_1\left(1+\left(\dfrac{\mu_{\mathrm{ep1}}E\sin\varphi}{\mu_{\mathrm{ap1}}E\cos\varphi+\bar{v}_{\mathrm{hd}}}\right)^2\right)+\dfrac{h^2E^2\sin^2\varphi}{105D_1}\left(\mu_{\mathrm{EOF}}+\dfrac{\mu_{\mathrm{ep1}}\bar{v}_{\mathrm{hd}}}{\mu_{\mathrm{ap1}}E\cos\varphi+\bar{v}_{\mathrm{hd}}}\right)\times\left(\left(\mu_{\mathrm{EOF}}+\dfrac{\mu_{\mathrm{ep1}}\bar{v}_{\mathrm{hd}}}{\mu_{\mathrm{ap1}}E\cos\varphi+\bar{v}_{\mathrm{hd}}}\right)\left(\dfrac{1}{2}-\left(\dfrac{3\Lambda}{5}+\dfrac{\Gamma_1}{3}\right)\right)-\mu_{\mathrm{ep1}}P_1\left(1-\dfrac{\mu_{\mathrm{ap1}}E\cos\varphi}{\mu_{\mathrm{ap1}}E\cos\varphi+\bar{v}_{\mathrm{hd}}}\right)\right)\right)}+\sqrt{\dfrac{w_0^{\,2}}{12}+\dfrac{2L}{\mu_{\mathrm{ap2}}E\cos\varphi+\bar{v}_{\mathrm{hd}}}\left(D_2\left(1+\left(\dfrac{\mu_{\mathrm{ep2}}E\sin\varphi}{\mu_{\mathrm{ap2}}E\cos\varphi+\bar{v}_{\mathrm{hd}}}\right)^2\right)+\dfrac{h^2E^2\sin^2\varphi}{105D_2}\left(\mu_{\mathrm{EOF}}+\dfrac{\mu_{\mathrm{ep2}}\bar{v}_{\mathrm{hd}}}{\mu_{\mathrm{ap2}}E\cos\varphi+\bar{v}_{\mathrm{hd}}}\right)\times\left(\left(\mu_{\mathrm{EOF}}+\dfrac{\mu_{\mathrm{ep2}}\bar{v}_{\mathrm{hd}}}{\mu_{\mathrm{ap2}}E\cos\varphi+\bar{v}_{\mathrm{hd}}}\right)\left(\dfrac{1}{2}-\left(\dfrac{3\Lambda}{5}+\dfrac{\Gamma_2}{3}\right)\right)-\mu_{\mathrm{ep2}}P_2\left(1-\dfrac{\mu_{\mathrm{ep2}}E\cos\varphi}{\mu_{\mathrm{ap2}}E\cos\varphi+\bar{v}_{\mathrm{hd}}}\right)\right)}\right)}$$

If Joule heating effects are negligible, our general equation for resolution in non-orthogonal micro free flow electrophoresis can be simplified as each of the terms Λ, Γ, and P become zero.

$$R_S = \frac{\left|\dfrac{\left(\mu_{\mathrm{ep1}}-\mu_{\mathrm{ep2}}\right)LE\sin\varphi\left(\mu_{\mathrm{EOF}}E\cos\varphi+\bar{v}_{\mathrm{hd}}\right)}{\left\{\left(\mu_{\mathrm{EOF}}+\mu_{\mathrm{ep1}}\right)E\cos\varphi+\bar{v}_{\mathrm{hd}}\right\}\left\{\left(\mu_{\mathrm{EOF}}+\mu_{\mathrm{ep2}}\right)E\cos\varphi+\bar{v}_{\mathrm{hd}}\right\}}\right|}{2\left(\sqrt{\dfrac{w_0^{\,2}}{12}+\dfrac{2L}{\left(\mu_{\mathrm{EOF}}+\mu_{\mathrm{ep1}}\right)E\cos\varphi+\bar{v}_{\mathrm{hd}}}\left(\dfrac{h^2}{210D_1}\left(\mu_{\mathrm{EOF}}+\dfrac{\mu_{\mathrm{ep1}}\bar{v}_{\mathrm{hd}}}{\left(\mu_{\mathrm{EOF}}+\mu_{\mathrm{ep1}}\right)E\cos\varphi+\bar{v}_{\mathrm{hd}}}\right)^2E^2\sin^2\varphi+D_1\left(1+\left(\dfrac{\mu_{\mathrm{ep1}}E\sin\varphi}{\left(\mu_{\mathrm{EOF}}+\mu_{\mathrm{ep1}}\right)E\cos\varphi+\bar{v}_{\mathrm{hd}}}\right)^2\right)\right)}}+\sqrt{\dfrac{w_0^{\,2}}{12}+\dfrac{2L}{\left(\mu_{\mathrm{EOF}}+\mu_{\mathrm{ep2}}\right)E\cos\varphi+\bar{v}_{\mathrm{hd}}}\left(\dfrac{h^2}{210D_2}\left(\mu_{\mathrm{EOF}}+\dfrac{\mu_{\mathrm{ep2}}\bar{v}_{\mathrm{hd}}}{\left(\mu_{\mathrm{EOF}}+\mu_{\mathrm{ep2}}\right)E\cos\varphi+\bar{v}_{\mathrm{hd}}}\right)^2E^2\sin^2\varphi+D_2\left(1+\left(\dfrac{\mu_{\mathrm{ep2}}E\sin\varphi}{\left(\mu_{\mathrm{EOF}}+\mu_{\mathrm{ep2}}\right)E\cos\varphi+\bar{v}_{\mathrm{hd}}}\right)^2\right)\right)}\right)}$$

$$= \frac{\left|\dfrac{\left(\mu_{\mathrm{ep1}}-\mu_{\mathrm{ep2}}\right)LE\sin\varphi\left(\mu_{\mathrm{EOF}}E\cos\varphi+\bar{v}_{\mathrm{hd}}\right)}{\left\{\left(\mu_{\mathrm{EOF}}+\mu_{\mathrm{ep1}}\right)E\cos\varphi+\bar{v}_{\mathrm{hd}}\right\}\left\{\left(\mu_{\mathrm{EOF}}+\mu_{\mathrm{ep2}}\right)E\cos\varphi+\bar{v}_{\mathrm{hd}}\right\}}\right|}{2\left(\sqrt{\dfrac{w_0^{\,2}}{12}+\dfrac{2DL}{\left(\mu_{\mathrm{EOF}}+\mu_{\mathrm{ep2}}\right)E\cos\varphi+\bar{v}_{\mathrm{hd}}}+\dfrac{2L\mu_{\mathrm{ep1}}^{\,2}E^2\sin^2\varphi}{\left\{\left(\mu_{\mathrm{EOF}}+\mu_{\mathrm{ep1}}\right)E\cos\varphi+\bar{v}_{\mathrm{hd}}\right\}^3}+\dfrac{2Lh^2E^2\sin^2\varphi}{210D_1\left(\mu_{\mathrm{EOF}}+\mu_{\mathrm{ep1}}\right)E\cos\varphi+\bar{v}_{\mathrm{hd}}}\left(\mu_{\mathrm{EOF}}+\dfrac{\mu_{\mathrm{ep1}}\bar{v}_{\mathrm{hd}}}{\left(\mu_{\mathrm{EOF}}+\mu_{\mathrm{ep1}}\right)E\cos\varphi+\bar{v}_{\mathrm{hd}}}\right)^2+}\sqrt{\dfrac{w_0^{\,2}}{12}+\dfrac{2D_2L}{\left(\mu_{\mathrm{EOF}}+\mu_{\mathrm{ep2}}\right)E\cos\varphi+\bar{v}_{\mathrm{hd}}}+\dfrac{2L\mu_{\mathrm{ep2}}^{\,2}E^2\sin^2\varphi}{\left\{\left(\mu_{\mathrm{EOF}}+\mu_{\mathrm{ep2}}\right)E\cos\varphi+\bar{v}_{\mathrm{hd}}\right\}^3}+\left(\dfrac{2Lh^2E^2\sin^2\varphi}{210D_2\left(\mu_{\mathrm{EOF}}+\mu_{\mathrm{ep2}}\right)E\cos\varphi+\bar{v}_{\mathrm{hd}}}\left(\mu_{\mathrm{EOF}}+\dfrac{\mu_{\mathrm{ep2}}\bar{v}_{\mathrm{hd}}}{\left(\mu_{\mathrm{EOF}}+\mu_{\mathrm{ep2}}\right)E\cos\varphi+\bar{v}_{\mathrm{hd}}}\right)^2\right)}\right)}$$

$$\therefore R_S = \frac{\left| \dfrac{\left(\mu_{\mathrm{ep1}} - \mu_{\mathrm{ep2}}\right) LE \sin\varphi \left(\mu_{\mathrm{EOF}} E\cos\varphi + \overline{v}_{\mathrm{hd}}\right)}{\left\{\left(\mu_{\mathrm{EOF}} + \mu_{\mathrm{ep1}}\right) E\cos\varphi + \overline{v}_{\mathrm{hd}}\right\}\left\{\left(\mu_{\mathrm{EOF}} + \mu_{\mathrm{ep2}}\right) E\cos\varphi + \overline{v}_{\mathrm{hd}}\right\}} \right|}{2\left(\begin{array}{l} \sqrt{\dfrac{w_0^{\,2}}{12} + \dfrac{2D_1 L}{\left(\mu_{\mathrm{EOF}} + \mu_{\mathrm{ep1}}\right) E\cos\varphi + \overline{v}_{\mathrm{hd}}} + \dfrac{2D_1 L \mu_{\mathrm{ep1}}^{\,2} E^2 \sin^2\varphi}{\left\{\left(\mu_{\mathrm{EOF}} + \mu_{\mathrm{ep2}}\right) E\cos\varphi + \overline{v}_{\mathrm{hd}}\right\}^3} + \dfrac{h^2 L E^2 \sin^2\varphi}{105 D_1 \left(\mu_{\mathrm{EOF}} + \mu_{\mathrm{ep1}}\right) E\cos\varphi + \overline{v}_{\mathrm{hd}}} \left(\mu_{\mathrm{EOF}} + \dfrac{\mu_{\mathrm{ep1}} \overline{v}_{\mathrm{hd}}}{\left(\mu_{\mathrm{EOF}} + \mu_{\mathrm{ep1}}\right) E\cos\varphi + \overline{v}_{\mathrm{hd}}} \right)^2} + \\ \sqrt{\dfrac{w_0^{\,2}}{12} + \dfrac{2D_2 L}{\left(\mu_{\mathrm{EOF}} + \mu_{\mathrm{ep2}}\right) E\cos\varphi + \overline{v}_{\mathrm{hd}}} + \dfrac{2D_2 L \mu_{\mathrm{ep2}}^{\,2} E^2 \sin^2\varphi}{\left\{\left(\mu_{\mathrm{EOF}} + \mu_{\mathrm{ep2}}\right) E\cos\varphi + \overline{v}_{\mathrm{hd}}\right\}^3} + \dfrac{h^2 L E^2 \sin^2\varphi}{105 D_2 \left(\mu_{\mathrm{EOF}} + \mu_{\mathrm{ep2}}\right) E\cos\varphi + \overline{v}_{\mathrm{hd}}} \left(\mu_{\mathrm{EOF}} + \dfrac{\mu_{\mathrm{ep2}} \overline{v}_{\mathrm{hd}}}{\left(\mu_{\mathrm{EOF}} + \mu_{\mathrm{ep2}}\right) E\cos\varphi + \overline{v}_{\mathrm{hd}}} \right)^2} \end{array} \right)}$$

2. Derivation of Equation 9 in main manuscript

Consider the non-orthogonal separation of two species with electrophoretic mobilities, μ_{ep1} and μ_{ep2} injected into a uniform electrical field E that makes an angle φ with the hydrodynamic flow of mean velocity, $\overline{v}_{\mathrm{hd}}$

Expressions for the average electrophoretic and average electroosmotic velocities in the direction perpendicular to (x direction) and parallel to the hydrodynamic flow (y direction) are:

$$\overline{v}_{\mathrm{ep},x} = \mu_{\mathrm{ep}} E \sin\varphi \qquad \overline{v}_{\mathrm{EOF},x} = 0$$

$$\overline{v}_{\mathrm{ep},y} = \mu_{\mathrm{ep}} E \cos\varphi \qquad \overline{v}_{\mathrm{EOF},y} = \mu_{\mathrm{EOF}} E \cos\varphi \,.$$

The average displacements of species during a residence time t are given by:

$$\overline{x} = (\overline{v}_{\mathrm{ep},x} + \overline{v}_{\mathrm{EOF},x})t = \mu_{\mathrm{ep}} E t \sin\varphi$$

$$\overline{y} = (\overline{v}_{\mathrm{ep},y} + \overline{v}_{\mathrm{EOF},y} + \overline{v}_{\mathrm{hd}})t = \left[(\mu_{\mathrm{ep}} + \mu_{\mathrm{EOF}}) E\cos\varphi + \overline{v}_{\mathrm{hd}} \right] t$$

For a separation channel of length L, the residence time is dependent on $\overline{v}_y$

$$t = \frac{L}{(\mu_{\mathrm{ep}} + \mu_{\mathrm{EOF}}) E\cos\varphi + \overline{v}_{\mathrm{hd}}}$$

$$\therefore t_1 = \frac{L}{(\mu_{\mathrm{ep1}} + \mu_{\mathrm{EOF}}) E\cos\varphi + \overline{v}_{\mathrm{hd}}} \text{ and } t_2 = \frac{L}{(\mu_{\mathrm{ep2}} + \mu_{\mathrm{EOF}}) E\cos\varphi + \overline{v}_{\mathrm{hd}}}$$

$$\therefore \overline{x}_1 = \frac{\mu_{\mathrm{ep1}} L E \sin\varphi}{(\mu_{\mathrm{ep1}} + \mu_{\mathrm{EOF}}) E\cos\varphi + \overline{v}_{\mathrm{hd}}} \text{ and } \overline{x}_2 = \frac{L E \sin\varphi}{(\mu_{\mathrm{ep2}} + \mu_{\mathrm{EOF}}) E\cos\varphi + \overline{v}_{\mathrm{hd}}}$$

$\overline{x}_1$ and $\overline{x}_2$ give the displacements of the centre of each separated stream.

The lateral separation is given by $\Delta x = \overline{x}_2 - \overline{x}_1$

$$\bar{x}_1 = \frac{\mu_{\mathrm{ep1}} LE \sin\varphi}{(\mu_{\mathrm{ep1}} + \mu_{\mathrm{EOF}})E\cos\varphi + \bar{v}_{\mathrm{hd}}} \text{ and } \bar{x}_2 = \frac{\mu_{\mathrm{ep2}} LE \sin\varphi}{(\mu_{\mathrm{ep2}} + \mu_{\mathrm{EOF}})E\cos\varphi + \bar{v}_{\mathrm{hd}}}$$

$$\therefore \Delta x = \frac{\mu_{\mathrm{ep2}} LE \sin\varphi}{(\mu_{\mathrm{ep2}} + \mu_{\mathrm{EOF}})E\cos\varphi + \bar{v}_{\mathrm{hd}}} - \frac{\mu_{\mathrm{ep1}} LE \sin\varphi}{(\mu_{\mathrm{ep1}} + \mu_{\mathrm{EOF}})E\cos\varphi + \bar{v}_{\mathrm{hd}}}$$

$$= \frac{\mu_{\mathrm{ep2}} LE \sin\varphi\left[(\mu_{\mathrm{ep1}} + \mu_{\mathrm{EOF}})E\cos\varphi + \bar{v}_{\mathrm{hd}}\right] - \mu_{\mathrm{ep1}} LE \sin\varphi\left[(\mu_{\mathrm{ep2}} + \mu_{\mathrm{EOF}})E\cos\varphi + \bar{v}_{\mathrm{hd}}\right]}{\left[(\mu_{\mathrm{ep2}} + \mu_{\mathrm{EOF}})E\cos\varphi + \bar{v}_{\mathrm{hd}}\right]\left[(\mu_{\mathrm{ep1}} + \mu_{\mathrm{EOF}})E\cos\varphi + \bar{v}_{\mathrm{hd}}\right]}$$

$$= \frac{\begin{array}{c}\mu_{\mathrm{ep1}}\mu_{\mathrm{ep2}} LE^2 \sin\varphi\cos\varphi + \mu_{\mathrm{EOF}}\mu_{\mathrm{ep2}} LE^2 \sin\varphi\cos\varphi + \mu_{\mathrm{ep2}} LE\bar{v}_{\mathrm{hd}} \sin\varphi \\ -\mu_{\mathrm{ep1}}\mu_{\mathrm{ep2}} LE^2 \sin\varphi\cos\varphi - \mu_{\mathrm{EOF}}\mu_{\mathrm{ep1}} LE^2 \sin\varphi\cos\varphi - \mu_{\mathrm{ep1}} LE\bar{v}_{\mathrm{hd}} \sin\varphi\end{array}}{\left[(\mu_{\mathrm{ep2}} + \mu_{\mathrm{EOF}})E\cos\varphi + \bar{v}_{\mathrm{hd}}\right]\left[(\mu_{\mathrm{ep1}} + \mu_{\mathrm{EOF}})E\cos\varphi + \bar{v}_{\mathrm{hd}}\right]}$$

$$= \frac{\mu_{\mathrm{EOF}} LE^2 \sin\varphi\cos\varphi(\mu_{\mathrm{ep2}} - \mu_{\mathrm{ep1}}) + (\mu_{\mathrm{ep2}} - \mu_{\mathrm{ep1}})LE\bar{v}_{\mathrm{hd}} \sin\varphi}{\left[(\mu_{\mathrm{ep2}} + \mu_{\mathrm{EOF}})E\cos\varphi + \bar{v}_{\mathrm{hd}}\right]\left[(\mu_{\mathrm{ep1}} + \mu_{\mathrm{EOF}})E\cos\varphi + \bar{v}_{\mathrm{hd}}\right]}$$

$$= \frac{(\mu_{\mathrm{ep2}} - \mu_{\mathrm{ep1}})LE \sin\varphi\left(\mu_{\mathrm{EOF}} E\cos\varphi + \bar{v}_{\mathrm{hd}}\right)}{\left[(\mu_{\mathrm{ep2}} + \mu_{\mathrm{EOF}})E\cos\varphi + \bar{v}_{\mathrm{hd}}\right]\left[(\mu_{\mathrm{ep1}} + \mu_{\mathrm{EOF}})E\cos\varphi + \bar{v}_{\mathrm{hd}}\right]}$$

3. Factors affecting resolution in non-orthogonal μFFE

3.1. Resolution of small positively charged molecules at elevated hydrodynamic flow rates

Small molecules are less affected by hydrodynamic dispersion than larger molecules, which diffuse more slowly. This means that the range of electroosmotic mobilities that enable baseline resolution to be achieved is much less restrictive with a resulting increase in the range of hydrodynamic velocities that can be used. In non-orthogonal μFFE, if $\mu_{\mathrm{EOF}} < 0$ the electroosmotic flow has its y component in the same direction as the hydrodynamic flow. Given that the best resolution occurs if $\bar{v}_y \sim 0$ with $\bar{v}_y > 0$, relatively slow hydrodynamic flow rates are favoured for $\mu_{\mathrm{EOF}} < 0$ (see Fig. 4B in the main text). By suppressing the electroosmotic mobility, $\bar{v}_y$ becomes negative unless a larger hydrodynamic velocity is used. The means that the baseline separation can be achieved at higher flow rates by manipulating the electroosmotic mobility so that the $v_{\mathrm{EOF,y}}$ is reduced in the direction of the hydrodynamic flow.

This concept is illustrated in **Fig. S1**. The hydrodynamic velocity used is almost four times larger than the maximum useful hydrodynamic velocity in Fig. 4B; however, baseline resolution is possible if $-1.2 \times 10^{-8}\ \mathrm{m^2 s^{-1} V^{-1}} < \mu_{\mathrm{EOF}} < -6 \times 10^{-9}\ \mathrm{m^2 s^{-1} V^{-1}}$ using appropriate values of φ.

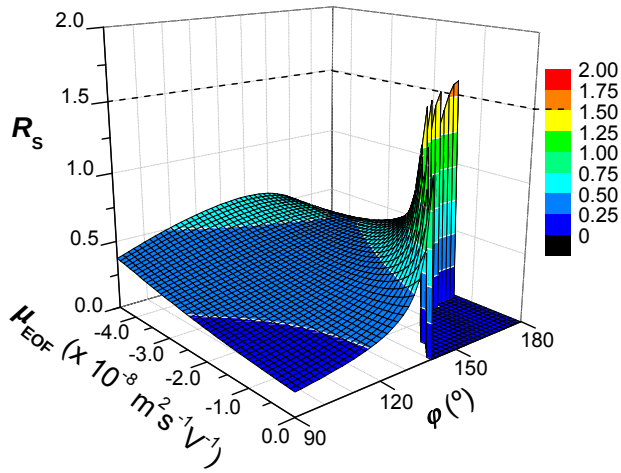

Figure S1: The variation of resolution with electroosmotic mobility and φ for small molecules using an elevated flow rate. The conditions used were: $\overline{v}_{hd}$ = 1.5 × 10^{-3} ms^{-1}, E = 3.6 × 10^4 Vm^{-1} and the electroosmotic mobility was varied from −4.5 × 10^{-8} to 0 $m^2s^{-1}V^{-1}$. The small molecules had electrophoretic mobilities of μ_{ep1} = 5.493 × 10^{-8} and μ_{ep} = 5.542 × 10^{-8} $m^2s^{-1}V^{-1}$, respectively.

3.2. The variation of resolution with electroosmotic mobility for large and small molecules

Figure S2A demonstrates the key role of electroosmotic mobility in the resolution of large molecules. As $\mu_{EOF} \rightarrow -\mu_{ep1}$ ($\mu_{ep1} < \mu_{ep2}$), there is a sharp increase in resolution for all values of φ due to the decrease in hydrodynamic dispersion. The more modest improvements for reduced electroosmotic mobilities and large values of φ are due to improved separation as $v_y \rightarrow 0$. The spiky appearance of the plot reflects the onset of sensitivity when a small change in μ_{EOF} or φ can result in v_y becoming negative. **Figure S2B** shows the corresponding plot for small ions. The "cliff-like" appearance of the plot occurs for combinations of μ_{EOF} and φ that change the sign of v_y. The contrast in the shapes of the plots in **Fig. S2A** and **Fig. S2B**, for φ = 270º and φ = 90º respectively, corroborates the strong influence of electroosmotic mobility on hydrodynamic dispersion for large molecules.

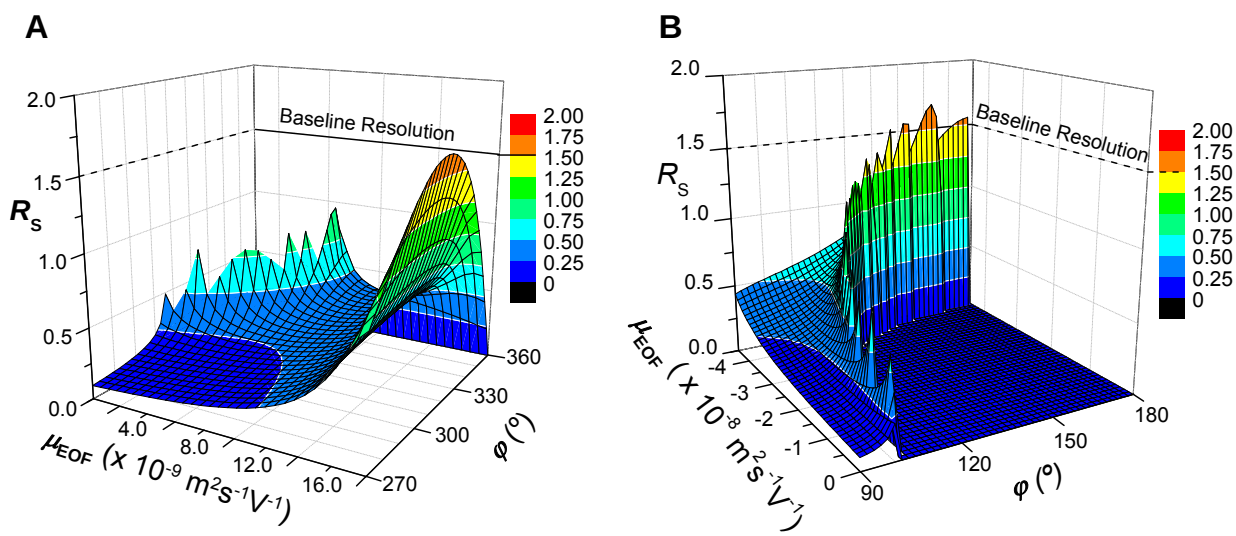

Figure S2. Variation of resolution with μ_{EOF} for: 2 large molecules (**A**), and two small molecules (**B**)
The conditions used were identical to those in **Fig. S1** except that the average hydrodynamic velocity was fixed ($\overline{v}_{hd}$ = 0.4 mms^{-1}) and in **A,** μ_{EOF} was varied from 0 to 1.8 × 10^{-8} $m^2s^{-1}V^{-1}$

4. The minimum difference in electrophoretic mobility that can be baseline resolved, $\mu_{\text{ep lim}}$

4.1. Derivation of a general equation for the minimum difference in electrophoretic mobility that can be baseline resolved, $\mu_{\text{ep lim}}$

The general expression for the resolution of two components by non-orthogonal μFFE is:

$$R_S = \frac{\left|\dfrac{\left(\mu_{\text{ep1}}-\mu_{\text{ep2}}\right)LE\sin\varphi\left(\mu_{\text{EOF}}E\cos\varphi+\bar{v}_{\text{hd}}\right)}{\left\{\left(\mu_{\text{EOF}}+\mu_{\text{ep1}}\right)E\cos\varphi+\bar{v}_{\text{hd}}\right\}\left\{\left(\mu_{\text{EOF}}+\mu_{\text{ep2}}\right)E\cos\varphi+\bar{v}_{\text{hd}}\right\}}\right|}{2\left(\sqrt{\dfrac{w_0^{\,2}}{12}+\dfrac{2L}{\left(\mu_{\text{EOF}}+\mu_{\text{ep1}}\right)E\cos\varphi+\bar{v}_{\text{hd}}}\left(D_1\left(1+\left(\dfrac{\mu_{\text{ep1}}E\sin\varphi}{\left(\mu_{\text{EOF}}+\mu_{\text{ep1}}\right)E\cos\varphi+\bar{v}_{\text{hd}}}\right)^2\right)+\dfrac{h^2E^2\sin^2\varphi}{105D_1}\left(\mu_{\text{EOF}}+\dfrac{\mu_{\text{ep1}}\bar{v}_{\text{hd}}}{\left(\mu_{\text{EOF}}+\mu_{\text{ep1}}\right)E\cos\varphi+\bar{v}_{\text{hd}}}\right)\times\left(\left(\mu_{\text{EOF}}+\dfrac{\mu_{\text{ep1}}\bar{v}_{\text{hd}}}{\left(\mu_{\text{EOF}}+\mu_{\text{ep1}}\right)E\cos\varphi+\bar{v}_{\text{hd}}}\right)\left(\dfrac{1}{2}-\left(\dfrac{3\Lambda}{5}+\dfrac{\Gamma_1}{3}\right)\right)-\mu_{\text{ep1}}P_1\left(1-\dfrac{\mu_{\text{ep1}}E\cos\varphi}{\left(\mu_{\text{EOF}}+\mu_{\text{ep1}}\right)E\cos\varphi+\bar{v}_{\text{hd}}}\right)\right)\right)}}+\sqrt{\dfrac{w_0^{\,2}}{12}+\dfrac{2L}{\left(\mu_{\text{EOF}}+\mu_{\text{ep2}}\right)E\cos\varphi+\bar{v}_{\text{hd}}}\left(D_2\left(1+\left(\dfrac{\mu_{\text{ep2}}E\sin\varphi}{\left(\mu_{\text{EOF}}+\mu_{\text{ep2}}\right)E\cos\varphi+\bar{v}_{\text{hd}}}\right)^2\right)+\dfrac{h^2E^2\sin^2\varphi}{105D_2}\left(\mu_{\text{EOF}}+\dfrac{\mu_{\text{ep2}}\bar{v}_{\text{hd}}}{\left(\mu_{\text{EOF}}+\mu_{\text{ep2}}\right)E\cos\varphi+\bar{v}_{\text{hd}}}\right)\times\left(\left(\mu_{\text{EOF}}+\dfrac{\mu_{\text{ep2}}\bar{v}_{\text{hd}}}{\left(\mu_{\text{EOF}}+\mu_{\text{ep2}}\right)E\cos\varphi+\bar{v}_{\text{hd}}}\right)\left(\dfrac{1}{2}-\left(\dfrac{3\Lambda}{5}+\dfrac{\Gamma_2}{3}\right)\right)-\mu_{\text{ep2}}P_2\left(1-\dfrac{\mu_{\text{ep2}}E\cos\varphi}{\left(\mu_{\text{EOF}}+\mu_{\text{ep2}}\right)E\cos\varphi+\bar{v}_{\text{hd}}}\right)\right)\right)}\right)} \qquad \text{Eq. S- 1}$$

The criterion for baseline resolution is $R_S = 1.50$. If we set $R_S = 1.50$, the minimum difference in electrophoretic mobility that can be baseline resolved, $\Delta\mu_{\text{ep lim}}$, can be calculated. We will assume that the electrophoretic mobilities, diffusion coefficients and dimensionless constants for the substances to be separated are very similar, so that $\mu_{\text{ep1}} \simeq \mu_{\text{ep2}} = \mu_{\text{ep}}$, $D_1 \simeq D_2 = D$, $\Gamma_1 \simeq \Gamma_2 = \Gamma$ and $P_1 \simeq P_2 = P$.

$$\therefore 1.50 = \frac{\left|\dfrac{\Delta\mu_{\text{ep lim}}LE\sin\varphi\left(\mu_{\text{EOF}}E\cos\varphi+\bar{v}_{\text{hd}}\right)}{\left\{\left(\mu_{\text{EOF}}+\mu_{\text{ep}}\right)E\cos\varphi+\bar{v}_{\text{hd}}\right\}^2}\right|}{4\left(\sqrt{\dfrac{w_0^{\,2}}{12}+\dfrac{2L}{\left(\mu_{\text{EOF}}+\mu_{\text{ep}}\right)E\cos\varphi+\bar{v}_{\text{hd}}}\left(D\left(1+\left(\dfrac{\mu_{\text{ep}}E\sin\varphi}{\left(\mu_{\text{EOF}}+\mu_{\text{ep}}\right)E\cos\varphi+\bar{v}_{\text{hd}}}\right)^2\right)+\dfrac{h^2E^2\sin^2\varphi}{105D}\left(\mu_{\text{EOF}}+\dfrac{\mu_{\text{ep}}\bar{v}_{\text{hd}}}{\left(\mu_{\text{EOF}}+\mu_{\text{ep}}\right)E\cos\varphi+\bar{v}_{\text{hd}}}\right)\times\left(\left(\mu_{\text{EOF}}+\dfrac{\mu_{\text{ep}}\bar{v}_{\text{hd}}}{\left(\mu_{\text{EOF}}+\mu_{\text{ep}}\right)E\cos\varphi+\bar{v}_{\text{hd}}}\right)\left(\dfrac{1}{2}-\left(\dfrac{3\Lambda}{5}+\dfrac{\Gamma}{3}\right)\right)-\mu_{\text{ep}}P\left(1-\dfrac{\mu_{\text{ep}}E\cos\varphi}{\left(\mu_{\text{EOF}}+\mu_{\text{ep}}\right)E\cos\varphi+\bar{v}_{\text{hd}}}\right)\right)\right)}\right)}$$

$$\therefore \left|\frac{\Delta\mu_{\text{ep lim}}LE\sin\varphi\left(\mu_{\text{EOF}}E\cos\varphi+\bar{v}_{\text{hd}}\right)}{\left\{\left(\mu_{\text{EOF}}+\mu_{\text{ep}}\right)E\cos\varphi+\bar{v}_{\text{hd}}\right\}^2}\right| = 6\left(\sqrt{\frac{w_0^{\,2}}{12}+\frac{2L}{\left(\mu_{\text{EOF}}+\mu_{\text{ep}}\right)E\cos\varphi+\bar{v}_{\text{hd}}}\left(\begin{array}{l}D\left(1+\left(\dfrac{\mu_{\text{ep}}E\sin\varphi}{\left(\mu_{\text{EOF}}+\mu_{\text{ep}}\right)E\cos\varphi+\bar{v}_{\text{hd}}}\right)^2\right)\\+\dfrac{h^2E^2\sin^2\varphi}{105D}\left(\mu_{\text{EOF}}+\dfrac{\mu_{\text{ep}}\bar{v}_{\text{hd}}}{\left(\mu_{\text{EOF}}+\mu_{\text{ep}}\right)E\cos\varphi+\bar{v}_{\text{hd}}}\right)\times\\\left(\left(\mu_{\text{EOF}}+\dfrac{\mu_{\text{ep}}\bar{v}_{\text{hd}}}{\left(\mu_{\text{EOF}}+\mu_{\text{ep}}\right)E\cos\varphi+\bar{v}_{\text{hd}}}\right)\left(\dfrac{1}{2}-\left(\dfrac{3\Lambda}{5}+\dfrac{\Gamma}{3}\right)\right)\right.\\\left.-\mu_{\text{ep}}P\left(1-\dfrac{\mu_{\text{ep}}E\cos\varphi}{\left(\mu_{\text{EOF}}+\mu_{\text{ep}}\right)E\cos\varphi+\bar{v}_{\text{hd}}}\right)\right)\end{array}\right)}\right)$$

$$\therefore \Delta\mu_{\mathrm{ep\,lim}} = \sqrt{\frac{3w_0^{\,2}\left\{\left(\mu_{\mathrm{EOF}}+\mu_{\mathrm{ep}}\right)E\cos\varphi+\overline{v}_{\mathrm{hd}}\right\}^4}{L^2E^2\sin^2\varphi\left(\mu_{\mathrm{EOF}}E\cos\varphi+\overline{v}_{\mathrm{hd}}\right)^2}+\frac{72\left\{\left(\mu_{\mathrm{EOF}}+\mu_{\mathrm{ep}}\right)E\cos\varphi+\overline{v}_{\mathrm{hd}}\right\}^3}{LE^2\sin^2\varphi\left(\mu_{\mathrm{EOF}}E\cos\varphi+\overline{v}_{\mathrm{hd}}\right)^2}\left(\begin{array}{l} D\left(1+\left(\frac{\mu_{\mathrm{ep}}E\sin\varphi}{\left(\mu_{\mathrm{EOF}}+\mu_{\mathrm{ep}}\right)E\cos\varphi+\overline{v}_{\mathrm{hd}}}\right)^2\right) \\ +\frac{h^2E^2\sin^2\varphi}{105D}\left(\mu_{\mathrm{EOF}}+\frac{\mu_{\mathrm{ep1}}\overline{v}_{\mathrm{hd}}}{\left(\mu_{\mathrm{EOF}}+\mu_{\mathrm{ep}}\right)E\cos\varphi+\overline{v}_{\mathrm{hd}}}\right)\times \\ \left(\left(\mu_{\mathrm{EOF}}+\frac{\mu_{\mathrm{ep1}}\overline{v}_{\mathrm{hd}}}{\left(\mu_{\mathrm{EOF}}+\mu_{\mathrm{ep}}\right)E\cos\varphi+\overline{v}_{\mathrm{hd}}}\right)\left(\frac{1}{2}-\left(\frac{3\Lambda}{5}+\frac{\Gamma}{3}\right)\right)\right. \\ \left.-\mu_{\mathrm{ep}}P\left(1-\frac{\mu_{\mathrm{ep}}E\cos\varphi}{\left(\mu_{\mathrm{EOF}}+\mu_{\mathrm{ep}}\right)E\cos\varphi+\overline{v}_{\mathrm{hd}}}\right)\right) \end{array}\right)}$$

$$\therefore \Delta\mu_{\mathrm{ep\,lim}} = \sqrt{\frac{3w_0^{\,2}\left\{\left(\mu_{\mathrm{EOF}}+\mu_{\mathrm{ep}}\right)E\cos\varphi+\overline{v}_{\mathrm{hd}}\right\}^4}{L^2E^2\sin^2\varphi\left(\mu_{\mathrm{EOF}}E\cos\varphi+\overline{v}_{\mathrm{hd}}\right)^2}+\frac{72D\left\{\left(\mu_{\mathrm{EOF}}+\mu_{\mathrm{ep}}\right)E\cos\varphi+\overline{v}_{\mathrm{hd}}\right\}^3}{LE^2\sin^2\varphi\left(\mu_{\mathrm{EOF}}E\cos\varphi+\overline{v}_{\mathrm{hd}}\right)^2}+\frac{72\mu_{\mathrm{ep}}^{\,2}D\left\{\left(\mu_{\mathrm{EOF}}+\mu_{\mathrm{ep}}\right)E\cos\varphi+\overline{v}_{\mathrm{hd}}\right\}}{L\left(\mu_{\mathrm{EOF}}E\cos\varphi+\overline{v}_{\mathrm{hd}}\right)^2}+\frac{72h^2\left\{\left(\mu_{\mathrm{EOF}}+\mu_{\mathrm{ep}}\right)E\cos\varphi+\overline{v}_{\mathrm{hd}}\right\}^3}{105DL\left(\mu_{\mathrm{EOF}}E\cos\varphi+\overline{v}_{\mathrm{hd}}\right)^2}\left(\begin{array}{l} \left(\mu_{\mathrm{EOF}}+\frac{\mu_{\mathrm{ep}}\overline{v}_{\mathrm{hd}}}{\left(\mu_{\mathrm{EOF}}+\mu_{\mathrm{ep}}\right)E\cos\varphi+\overline{v}_{\mathrm{hd}}}\right)\times \\ \left(\left(\mu_{\mathrm{EOF}}+\frac{\mu_{\mathrm{ep}}\overline{v}_{\mathrm{hd}}}{\left(\mu_{\mathrm{EOF}}+\mu_{\mathrm{ep}}\right)E\cos\varphi+\overline{v}_{\mathrm{hd}}}\right)\left(\frac{1}{2}-\left(\frac{3\Lambda}{5}+\frac{\Gamma}{3}\right)\right)\right. \\ \left.-\mu_{\mathrm{ep}}P\left(1-\frac{\mu_{\mathrm{ep}}E\cos\varphi}{\left(\mu_{\mathrm{EOF}}+\mu_{\mathrm{ep}}\right)E\cos\varphi+\overline{v}_{\mathrm{hd}}}\right)\right) \end{array}\right)} \qquad \text{Eq. S- 2}$$

When the temperature difference in the channel is small enough to have a negligible influence on resolution, this expression simplifies to:

$$\therefore \Delta\mu_{\mathrm{ep\ \ lim}} = \sqrt{\frac{3w^2\left\{\left(\mu_{\mathrm{EOF}}+\mu_{\mathrm{ep}}\right)E\cos\varphi+\overline{v}_{\mathrm{hd}}\right\}^4}{L^2E^2\sin^2\varphi\left(\mu_{\mathrm{EOF}}E\cos\varphi+\overline{v}_{\mathrm{hd}}\right)^2}+\frac{72D\left\{\left(\mu_{\mathrm{EOF}}+\mu_{\mathrm{ep}}\right)E\cos\varphi+\overline{v}_{\mathrm{hd}}\right\}^3}{LE^2\sin^2\varphi\left(\mu_{\mathrm{EOF}}E\cos\varphi+\overline{v}_{\mathrm{hd}}\right)^2}+\frac{72D\mu_{\mathrm{ep}}^{\,2}\left\{\left(\mu_{\mathrm{EOF}}+\mu_{\mathrm{ep}}\right)E\cos\varphi+\overline{v}_{\mathrm{hd}}\right\}}{L\left(\mu_{\mathrm{EOF}}E\cos\varphi+\overline{v}_{\mathrm{hd}}\right)^2}+\frac{36h^2\left\{\left(\mu_{\mathrm{EOF}}+\mu_{\mathrm{ep}}\right)E\cos\varphi+v_{\mathrm{hd}}\right\}^3}{105DL\left(\mu_{\mathrm{EOF}}E\cos\varphi+\overline{v}_{\mathrm{hd}}\right)^2}\left(\mu_{\mathrm{EOF}}+\frac{\mu_{\mathrm{ep}}v_{\mathrm{hd}}}{\left(\mu_{\mathrm{EOF}}+\mu_{\mathrm{ep}}\right)E\cos\varphi+v_{\mathrm{hd}}}\right)^2} \qquad \text{Eq. S- 3}$$

For orthogonal μFFE, the corresponding general expression simplifies to:

$$\therefore \Delta\mu_{\mathrm{ep\,lim}} = \sqrt{\frac{3w_0^{\,2}\overline{v}_{\mathrm{hd}}^{\,2}}{L^2E^2}+\frac{72D\overline{v}_{\mathrm{hd}}}{LE^2}+\frac{72\mu_{\mathrm{ep}}^{\,2}D}{L\overline{v}_{\mathrm{hd}}}+\frac{72h^2\overline{v}_{\mathrm{hd}}}{105DL}\left(\left(\mu_{\mathrm{EOF}}+\mu_{\mathrm{ep}}\right)\times\left(\left(\mu_{\mathrm{EOF}}+\mu_{\mathrm{ep}}\right)\left(\frac{1}{2}-\left(\frac{3\Lambda}{5}+\frac{\Gamma_1}{3}\right)\right)-\mu_{\mathrm{ep}}P\right)\right)} \qquad \text{Eq. S- 4}$$

and when Joule heating effects are negligible,

$$\Delta\mu_{\mathrm{ep\ \ lim}} = \sqrt{\frac{3w_0^{\,2}\overline{v}_{\mathrm{hd}}^{\,2}}{L^2E^2}+\frac{72D\overline{v}_{\mathrm{hd}}}{LE^2}+\frac{72D\mu_{\mathrm{ep}}^{\,2}}{L\overline{v}_{\mathrm{hd}}}+\frac{36h^2\overline{v}_{\mathrm{hd}}\left(\mu_{\mathrm{EOF}}+\mu_{\mathrm{ep}}\right)^2}{105DL}} \qquad \text{Eq. S- 5}$$

4.2. Plots of the variation of $\mu_{\text{ep lim}}$ *vs* E for large and small molecules

Figure S-3 shows how the resolving power, measured by $\Delta\mu_{\text{ep lim}}$, of the molecules described in **Fig. S2** varies with E and φ for two hydrodynamic velocities. The shape of the plot in **Fig. S3A** is similar in shape to the mirror image of **Fig. 3A** in the main text. This is to be expected as the smallest difference in electrophoretic mobility that can be resolved occurs for conditions which give the best resolution. For conditions in which Joule heating is not problematic, increasing the electrical field strength reduces the size of $\Delta\mu_{\text{ep lim}}$ for all values of φ. Using orthogonal μFFE for the conditions described and a field strength of 3.6×10^4 Vm^{-1}, the minimum difference in electrophoretic mobility that can be resolved is 2.90×10^{-10} $\text{m}^2\text{s}^{-1}\text{V}^{-1}$ which corresponds to more than 1.5% of the electrophoretic mobility of the species involved. $\Delta\mu_{\text{ep lim}}$ can be reduced to a value of 1.54×10^{-10} $\text{m}^2\text{s}^{-1}\text{V}^{-1}$ by setting φ to 138º; i.e.

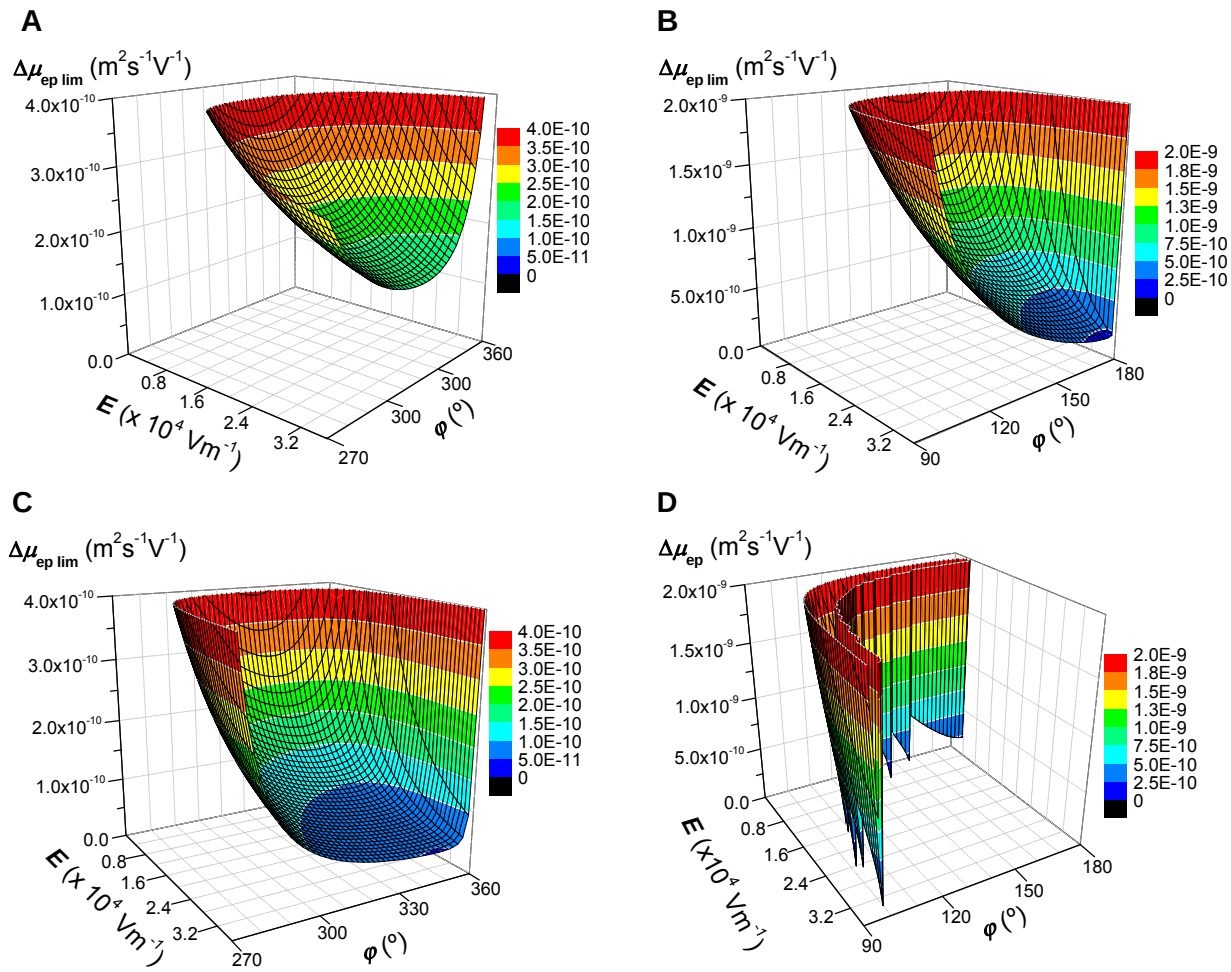

FigureS3: Variation of the minimum difference in electrophoretic mobility that can be resolved with E and φ, for two hydrodynamic velocities for large molecules (**A**) and (**C**) and for small molecules (**B**) and (**D**). The hydrodynamic velocities are: $\bar{v}_{\text{hd}} = 4 \times 10^{-4}$ ms^{-1} in **A** and **B** and $\bar{v}_{\text{hd}} = 5 \times 10^{-5}$ ms^{-1} in (**C**) and (**D**). The electrophoretic mobilities and electroosmotic mobility used for the large molecules are: $\mu_{\text{ep1}} = -1.813 \times 10^{-8}$, $\mu_{\text{ep2}} = -1.832 \times 10^{-8}$, and $\mu_{\text{EOF}} = 1.80 \times 10^{-8}$ m^2s^{-1} V^{-1} in (**A**) and (**C**), respectively, and for the small molecules: $\mu_{\text{ep1}} = 5.493 \times 10^{-8}$, $\mu_{\text{ep2}} = 5.542 \times 10^{-8}$, and $\mu_{\text{EOF}} = -5.28 \times 10^{-8}$ $\text{m}^2\text{s}^{-1}\text{V}^{-1}$ in (**B**) and (**D**), respectively. The channel height used for each panel was h = 20 μm.

$\Delta\mu_{\text{ep lim}} < 0.01\ \mu_{\text{ep.}}$. **Fig. S3C** shows that further improvements to $\Delta\mu_{\text{ep lim}}$ can be made by reducing $\overline{v}_{\text{hd}}$ to 5×10^{-5} ms^{-1}, $\Delta\mu_{\text{ep lim}} < 5 \times 10^{-11}$ m^{2}s^{-1}V^{-1}; this is less than 0.3% of the electrophoretic mobility of the DNA fragments. The improvement in resolution comes from the greater difference in time that the molecules spend in the electrical field as $v_y \rightarrow 0$. The disadvantage of using such a low flow rate is the 8× reduction in the sample throughput.

Figure S3B has the same basic shape as **Fig. S3A** but the size of $\Delta\mu_{\text{ep lim}}$ is slightly larger with a minimum value $\Delta\mu_{\text{ep lim}} = 2.05 \times 10^{-10}$ m^{2}s^{-1}V^{-1} occurring at $E = 3.6 \times 10^4$ Vm^{-1} and $\varphi = 175°$. $\Delta\mu_{\text{ep lim}} \simeq 0.4\%$ of μ_{ep}. **Fig. S3D** demonstrates that for the small molecules, there is little advantage to be gained from using a lower hydrodynamic flow rate as v_y becomes negative for relatively low values of E and φ preventing both species from being collected. It is likely that any separation carried out under these conditions would be rather unstable as the surface plot is narrow and steep so that any small fluctuations in E or v_{hd} could have a significant impact on the quality of the separation.